# Parahippocampal and retrosplenial connections of rat posterior parietal cortex

Grethe M. Olsen[1], Shinya Ohara[2], Toshio Iijima[2] and Menno P. Witter[1, 3]

[1]Kavli Institute for Systems Neuroscience, Centre for Neural Computation, Egil and Pauline Braathen and Fred Kavli Centre for Cortical Microcircuits, NTNU – Norwegian University of Science and Technology, The Faculty of Medicine, Postbox 8905, 7491 Trondheim, Norway

[2]Division of Systems Neuroscience, Tohoku University Graduate School of Life Sciences, Katahira 2-1-1, Aoba-Ku, Sendai 980-8577, Japan

[3]Correspondence to Menno P. Witter, Kavli Institute for Systems Neuroscience, Medical-Technical Research Center, NTNU
Postbox 8905
NO-7491Trondheim
NORWAY
Phone: +47 73598249
Email: menno.witter@ntnu.no
[1]

Number of text pages: 51

Number of figures: 14

Number of tables: 0

Keywords: retrograde tracing, anterograde tracing, rabies virus tracing, immunohistochemistry, spatial navigation, AB_10073917, AB_2298772

[1] This study was supported by the Kavli Foundation and Centre of Excellence (#145993), equipment (#181676), and research (#191929) grants from the Norwegian Research Council.

**Abstract**

The posterior parietal cortex has been implicated in spatial functions, including navigation. The hippocampal and parahippocampal region and the retrosplenial cortex are crucially involved in navigational processes and connections between the parahippocampal/retrosplenial domain and the posterior parietal cortex have been described. However, an integrated account of the organization of these connections is lacking. Here we investigated parahippocampal connections of each posterior parietal subdivision and the neighboring secondary visual cortex using conventional retrograde and anterograde tracers as well as transsynaptic retrograde tracing with a modified rabies virus. The results show that posterior parietal as well as secondary visual cortex entertain overall sparse connections with the parahippocampal region but not with the hippocampal formation. The medial and lateral dorsal subdivisions of posterior parietal cortex receive sparse input from deep layers of all parahippocampal areas. Conversely, all posterior parietal subdivisions project moderately to dorsal presubiculum, whereas rostral perirhinal cortex, postrhinal cortex, caudal entorhinal cortex and parasubiculum all receive sparse posterior parietal input. This indicated that the presubiculum might be a major liaison between parietal and parahippocampal domains. In view of the close association of the presubiculum with the retrosplenial cortex, we included the latter in our analysis. Our data indicate that posterior parietal cortex is moderately connected with the retrosplenial cortex, particularly with rostral area 30. The relative sparseness of the connectivity with the parahippocampal and retrosplenial domains suggests that posterior parietal cortex is only a modest actor in forming spatial representations underlying navigation and spatial memory in parahippocampal and retrosplenial cortex.

## Introduction

Since the discovery of place cells in the rat hippocampus (O'Keefe and Dostrovsky, 1971), the hippocampal formation and the associated parahippocampal region (PHR), have undergone extensive experimental investigation with a strong focus on cell types and networks relevant for navigation. The PHR consists of several distinct subareas, in rats comprising the peri-, post- and entorhinal cortices, as well as the pre- and parasubiculum. Neurons in several of these parahippocampal areas have spatial properties. For instance, the presubiculum (PrS), parasubiculum (PaS), and the medial entorhinal cortex (MEC) contain head-direction cells, grid cells, and border cells (Taube et al., 1990a; Taube, 1995; Fyhn et al., 2004; Hafting et al., 2005; Sargolini et al., 2006; Solstad et al., 2008; Boccara et al., 2010). In addition, MEC contains cells responding to the animal's running speed (Kropff et al., 2015). Moreover, lesions of these areas lead to impairments in tasks that test spatial memory (Morris et al., 1982; Taube et al., 1992; Jarrard et al., 2004; Steffenach et al., 2005). The retrosplenial cortex (RSC) is reciprocally connected with several areas in the PHR (van Groen and Wyss, 1990a; b; c; 1992; 2003; Burwell and Amaral, 1998a; Jones and Witter, 2007; Agster and Burwell, 2009; Kononenko and Witter, 2012; Czajkowski et al., 2013; Sugar and Witter, 2016) and shares some functional properties with spatially and directionally modulated neurons in MEC, PrS and PaS (Chen et al., 1994; Cho and Sharp, 2001; Alexander and Nitz, 2015).

The rat posterior parietal cortex (PPC) is a higher order, multimodal association area which has been proposed to be involved in numerous functions, including spatial navigation, decision making and directed attention. Lesion studies from several groups in the 1980's described spatial

deficits in PPC-lesioned animals, particularly in water maze tasks, with the most common impairment being an error in initial heading angle (Kolb et al., 1983; Kolb and Walkey, 1987; DiMattia and Kesner, 1988). Yet, although PPC-lesioned rats have inaccurate trajectories in the water maze, their behavior is clearly goal directed (Save and Poucet, 2000b). Despite these behavioral observations, data on spatial properties of neurons in PPC are sparse and inconsistent. Recording studies in freely behaving animals revealed cells with head directional properties in PPC (Chen et al., 1994). These cells were not as sharply directionally tuned as head direction cells in the simultaneously recorded RSC, but were to a larger extent behaviorally modulated, meaning that the directionality of a high proportion of PPC cells (57%) was associated with specific movements such as turns. In contrast, such an association was found in only a few cells in RSC area 30 (19%) and in no cells in RSC area 29. A more recent study confirmed that although cells in PPC were behaviorally modulated, being tuned to specific modes of movement, head directional responses were only sparsely observed and spatial coherence was weak (Whitlock et al., 2012). Additionally, the latter authors noticed that the properties of PPC cells changed according to task demands, being different if the rats ran in an open arena versus in a geometrically structured, so-called hairpin maze. If the rats ran hairpin-like sequences in an open arena, the firing patterns of cells in PPC were similar to those recorded when the rats ran in the actual hairpin maze, further confirming the behavioral modulation of these cells. Other studies have found that modulation of PPC neurons depends on the position of the animal in a labyrinth- or spiral-like maze (Nitz, 2006; 2012), or the direction to a goal relative to the animal's head (Wilber et al., 2014). It has therefore been suggested that PPC integrates internal information about self-motion with external information about spatial location in order to guide navigation (for review, see for instance Whitlock et al., 2008; Save and Poucet, 2009; Whitlock, 2014). One

may thus hypothesize that PPC and PHR might be connected and, indeed, previous studies have described direct connections but indicated that they are sparse (Reep et al., 1994; Burwell and Amaral, 1998a; Agster and Burwell, 2009). However, these studies did not investigate whether different subdivisions of PPC might show variations in the strength of their connectivity with the PHR. A complicating factor has been that different delineations of PPC as a whole as well as of its subdivisions have been used, thus confounding the establishment of a generally accepted connectivity scheme. In a previous paper, we described a reliable way to assess borders in the parietal cortical domain and defined PPC and its three subdivisions (Olsen and Witter, 2016). In the current study, we set out to describe PPC connections with the parahippocampal and retrosplenial domain in detail, using anterograde and retrograde tracing methods.

## Materials and methods

### Tracer injections and histology

In total, 30 adult female Sprague Dawley rats (Charles River, Sulzfeld/Kisslegg, Germany; 180-230 g at the time of surgery) were used for the anterograde and retrograde tracing experiments. All experimental procedures followed locally approved protocols that adhere to national and EU regulations. The methods for tracer injections, perfusions and histology have been described in detail previously (Olsen and Witter, 2016). Briefly, under deep gas-induced anesthesia, rats were injected with retrograde and/or anterograde tracers (Fast Blue; Fluorogold; Diamidino Yellow; *Phaseolus vulgaris* Leucoagglutinin, PHA-L; and 10 kDa Biotinylated dextran amine, BDA). Injections were stereotactically placed, based on a stereotaxic atlas (Paxinos and Watson, 2007). We aimed to inject in medial, lateral and caudolateral subdivisions of PPC (mPPC, lPPC, and

PtP, respectively) as well as the medial and lateral divisions of the secondary visual cortex (V2M and V2L, respectively). Retrograde tracers were pressure injected into the brain through 1 µl Hamilton syringes. Iontophoretic injections of anterograde tracers were performed using glass micropipettes (alternating currents, 6 seconds on/6 seconds off, 6 µA for BDA and 7 µA for PHA-L). Upon completion of injections, the wound was cleaned and sutured, and the animal was put back in its home cage.

After a survival period of 1-2 weeks, animals were deeply anesthetized and perfused transcardially with a Ringer solution (pH 6.9, 37°C) followed by a solution of freshly depolymerized 4% paraformaldehyde in phosphate buffer (pH 7.4). The brains were extracted and postfixed overnight in the same fixative at 4°C. After being cryoprotected in a DMSO/glycerol solution at least overnight, six equally spaced series of 50 µm coronal sections were cut on a freezing microtome. One series was mounted on Superfrost plus-slides and stained with cresyl violet for cytoarchitectural orientation. For brains containing fluorescent retrograde tracers, one series was mounted on uncoated microscope slides for analysis of labeling without any further processing. For brains containing anterograde tracers, one series was stained for BDA and/or PHA-L using the fluorochromes AlexaFluor® 488 and AlexaFluor® 546. Sections were mounted on uncoated microscope slides, dried, dehydrated in increasing concentrations of ethanol and coverslipped using Entellan as mounting medium. For some brains, additional series were processed to visualize one of the anterograde tracers, using 3,3'-Diaminobenzidine tetrahydrochloride (DAB) as the chromogen.

The injection sites have been described in detail elsewhere (Olsen and Witter, 2016). Representative cases were selected for illustration of labeling patterns. For cases injected with retrograde tracers, mounted sections were investigated using a Carl Zeiss Axio Imager M2 microscope (Carl Zeiss Microscopy, Jena, Germany) with reflected fluorescent light of appropriate wavelength, connected to a camera that allowed to display a live image on the computer screen. The outline of selected sections and the distribution of retrogradely labeled neurons were mapped using Neurolucida (MicroBrightField, Colchester, VT). Using Adobe Illustrator CS6 (Adobe Systems Incorporated, San Jose, CA), these Neurolucida images were overlaid with images of Nissl stained sections at the corresponding level from the same brain to delineate subdivisions of PHR and RSC and to represent the distribution of labeled neurons within them.

Cases with injections of anterograde tracers were scanned using a Mirax-midi scanner (objective 20X, NA 0.8; Carl Zeiss Microscopy), using either reflected fluorescence (for sections stained with a fluorophore) or transmitted white light (for sections stained with DAB and/or Cresyl Violet) as the light source. Pictures of the regions of interest were exported as high resolution tif-files, cropped and adjusted in Adobe Photoshop CS6 (Adobe Systems Incorporated). For analysis of labeled fibers in the PHR, the pictures were converted to PNG files, while for analysis of labeled fibers in RSC brightness and contrast were adjusted. Subsequently, the pictures were imported into Adobe Illustrator, where they were overlaid with images of Nissl stained sections at the corresponding level from the same brain in which borders had been outlined for the regions of interest. In such maps of PHR, anterogradely labeled fibers were traced.

Virus injections and histology

These experiments were performed in the laboratory of Dr. T. Iijima at the Tohoku University in Sendai, Japan, under the supervision of Dr. S. Ohara. Subjects were seven male adult Wistar rats (Kumagai-shigeyasu Co., Ltd, Miyagi, Japan) weighing 210-250 g at the time of surgery. Before surgery, animals were injected intraperitoneally with ketamine (60 mg/kg, Daiichi Sankyo Co., LTD, Tokyo, Japan) and xylazine (4.8 mg/kg, Bayer Yakuhin LTD, Osaka, Japan) to induce general anesthesia, as well as Atropine Sulfate (0.5 mg/kg, Mitshubishi Tanabe Pharma, Osaka, Japan). In order to maintain the anesthesia, additional doses of ketamine were administered intramuscularly every 20-30 minutes during the surgery. Under sterile conditions, deeply anesthetized rats were fixed in a stereotaxic frame (Narishige, Tokyo, Japan). An incision of the skin was made along the midline of the skull, the skin was retracted and a burr hole was drilled at the appropriate coordinate using the midsagital and transverse sinuses as reference points. A previously described genetically modified rabies virus inserted with two genes for enhanced green fluorescent protein (EGFP) was used for transsynaptic retrograde tracing (rHEP5.0-CVSG-EGFPx2, 1.0x10^8 ffu/ml; mixed 9:1 with a 10% solution of the blue dye Pontamine Sky Blue, Avocado Research Chemicals Ltd, Lancashire, UK; see Inoue et al., 2004; Ohara et al., 2009). 100 nl virus/dye mix was pressure injected into the MEC of the right hemisphere through a glass micropipette fixed to a 1 µl Hamilton needle at a rate of 20 nl per minute. Upon completion of the injection, the pipette was left in place for an additional 15 minutes before being retracted from the skull. The burr hole was cleaned and filled first with Vaseline and then dental cement (GC Corporation, Tokyo, Japan) before the wound was cleaned and closed with clips (World Precision Instruments, Sarasota, FL). Each operated animal was put singly into a cage with

sufficient food and water for up to a week, and the cage was placed in a ventilated, enclosed biosafety cabinet. After a survival time of 2-5.5 days, animals were anesthetized and perfused transcardially in a ventilated hood with 10% sucrose followed by the 4% paraformaldehyde solution described above. The brains were extracted and postfixed in the same fixative, then cryoprotected in 30% sucrose until equilibrium. The brain hemispheres were split along the midsagital line, and using a freezing microtome (Leica Microsystems, Wetzlar, Germany), 50 µm sections were prepared in six equally spaced series. The injected hemisphere was cut sagitally, and the contralateral hemisphere was cut coronally.

For each hemisphere, one series was immunostained against green fluorescent protein (GFP) which was expressed in virus infected cells. Free floating sections were rinsed in phosphate buffered saline (PBS), blocked with 3% $H_2O_2$ for 10 minutes, rinsed in PBS, and incubated for 1 hour in immunobuffer (PBS containing 5% normal goat serum, 0.05% $NaN_3$, and 0.1% Triton X-100). Next, the sections were incubated with rabbit anti-GFP (1:3000; Invitrogen, Molecular Probes, Eugene, OR; cat# A11122, RRID:AB_10073917) in immunobuffer for 20 hours at 4°C and rinsed in PBS containing 0.1% Triton X-100 (PBT). With rinses in between, the sections were subsequently incubated with biotinylated goat anti-rabbit (Jackson Immuno Research Laboratories, West Grove, PA) for 2 hours at room temperature, with ABC (Vector laboratories, Burlingame, CA) for 4 hours at room temperature, and finally with DAB intensified with Ammonium Nickel (II)-Chloride Hexahydrate (Wako, Osaka, Japan). After being rinsed with PBS, the sections were mounted on coated microscope slides, dehydrated in increasing concentrations of ethanol and coverslipped using VectaMount AQ Aqueous Mounting Medium (Vector laboratories). To obtain cytoarchitectural delineations, one series of each brain was Nissl

stained using Thionin or stained for neuronal nuclei using a standard immunohistochemical protocol with DAB as the final reaction product (primary antibody mouse anti-NeuN 1:1000, Millipore, Billerica, MA; cat# MAB 377, RRID:AB_2298772).

Stained sections were scanned using an automated Mirax-midi scanner with transmitted white light as the light source. For two representative cases, high resolution tif-images of the regions of interest were exported, and Adobe Photoshop was used to turn them into pseudo darkfield images for better contrast. The images were overlaid with pictures of adjacent NeuN stained sections in Adobe Illustrator and PPC was outlined.

## Results

### Delineation of target areas

In this paper we have investigated the connections of the PPC with the PHR and the closely associated RSC. We have previously described the three subdivisions of PPC in detail based on cytoarchitectural delineations and thalamic connections (Olsen and Witter, 2016). PPC is located dorsally in the brain, between the somatosensory and occipital domains, and contains a medial (mPPC), a lateral (lPPC) and a caudolateral (PtP) subdivision (Fig. 1a). In mPPC, lamination is poorly developed and cells are homogenously distributed throughout the cortex. The laterally adjacent lPPC appears more laminated, mainly due to layer 5 being slightly less populated. The most lateral and caudal subdivision, PtP, contains even fewer cells in layer 5, and weakly stained layer 3/4 cells in Nissl stained sections.

The rat PHR (Fig. 1b) comprises several distinct subareas, namely the perirhinal (PER), postrhinal (POR), and entorhinal (EC) cortices, as well as the presubiculum (PrS) and parasubiculum (PaS). PER can be further subdivided into a ventrally situated area 35 and a dorsally located area 36, while EC comprises a lateral and medial subdivision (LEC and MEC, respectively). To delineate the PHR, we relied on a recent description in which all subdivisions have been delineated in three standard planes, coronal, horizontal and sagittal (Boccara et al., 2015). We denominate the layers of PHR and RSC with roman numerals, whereas layers of neocortical areas are denominated with arabic numbers. PER is located on the banks and in the fundus of the rhinal fissure, and is overall poorly laminated. This is in contrast to its rostral neighbor the insular cortex, which has a striking trilaminar appearance, and overlies the claustrum. A distinguishing feature of area 35 is its large, darkly stained, heart-shaped pyramidal cells in layer V, while area 36 is characterized by a thick, bilaminate layer VI. Caudal to PER one finds POR, which for the most part is situated dorsal to the rhinal fissure. In coronal sections, POR emerges at the caudal pole of the angular bundle at a level where subicular cells are no longer visible. POR has an even poorer laminar organization than PER, and appears quite homogenous, although patches of layer II cells extend into layer I, giving the most superficial cell layer an irregular appearance. Dorsal to both PER and POR is the temporal cortex, which appears more laminated than its ventral neighbors. Ventral to PER and POR, EC is located, which sits dorsal and caudal to the piriform cortex. Although EC has been subdivided in several fields, we will use only the two main portions, LEC and MEC. A distinguishing feature of EC that is not seen in PER or POR is the cell sparse lamina dissecans between the middle cell layers III and V, as well as larger cells in layer II. The lamina dissecans is better developed in MEC

than LEC, in addition, LEC layer II contains smaller and more lightly Nissl stained cells that are not as densely packed as in MEC layer II. The lamina dissecans is also apparent in the adjacent PaS and PrS. In PaS, layers II and III merge and consist of large, lightly stained pyramidal cells. In ventral PrS, cells in superficial layers II and III are smaller than in PaS, and densely packed. The dorsal portion of PrS (named postsubiculum by some, for instance van Groen and Wyss, 1990c) is characterized by a thin layer II which contains small, darkly stained neurons that are grouped into clusters.

RSC constitutes the midline wall in the caudal half of the cerebrum (not shown) and is generally subdivided in two main portions (Sugar et al., 2011). In the ventrally situated granular portion (area 29), cells in layers II and III are small, granular and very densely packed. Layer V contains small-to-medium sized pyramidal cells. In the dorsally adjacent dysgranular RSC (area 30), superficial layers are wider, but layers II and III are still difficult to distinguish from each other. The pyramidal cells of layer V in area 30 are bigger than in area 29, and appear radially organized. In coronal sections, secondary motor cortex (M2) is positioned lateral to RSC at rostral levels. M2 layer 5 is more densely packed, and layers 2/3 are wider than in area 30. M2 is caudally replaced by the medial portion of secondary visual cortex (V2M), which protrudes more rostrally than the rest of the visual cortex. In coronal sections it first appears as a thin strip of cortex where cells are distributed homogeneously through the whole depth of the cortex and layers are poorly developed. The exact transition between M2 and V2M is difficult to discern in coronal sections. At levels caudal to the splenium of the corpus callosum, the ventrally neighboring PrS is distinguished from RSC by the characteristic lamina dissecans (see description above).

Retrograde tracing of projections from PHR to dorsal association areas

We analyzed 11 injections of retrograde tracers in the parietal and occipital domains of the cortex, seven of which were in PPC (four in mPPC, three in lPPC) and four in V2M. In all cases, retrogradely labeled cells were observed in several of the parahippocampal areas, with most of the labeled cells located in deep layers. The largest proportion of labeled cells was found in the hemisphere ipsilateral to the injection site. In general, cells in the PHR showed weaker labeling than cells in other areas of the cortex at the same rostrocaudal level (not illustrated).

*Injections in PPC*

After an injection of Fast Blue with its core placed rostrally in mPPC (Fig. 2), we observed retrogradely labeled cells mainly in deep layers of PHR. PER areas 36 and 35, and POR contained labeled cells in superficial layer VI as well as layer V along their full rostrocaudal extents (Fig. 2a-f), only occasionally were labeled cells found in superficial layers. In both PER and POR, labeled cells were distributed along the entire dorsoventral axis. In LEC and MEC, we noted sparsely distributed labeled cells superficially in layer V (Fig. 2a-e), throughout the rostrocaudal and mediolateral extents, but more densely clustered close to the rhinal fissure, dorsally in LEC as well as caudally in MEC. A few labeled cells were found in deep layers of dorsal PrS (not shown) and the ventral portion of PaS (Fig. 2e). In regions adjacent to PHR, a few labeled cells were seen in the banks and fundus of the rhinal fissure rostral to PER and LEC, in caudal portions of insular and piriform cortices (not shown). Notable labeling was also found in temporal cortical areas dorsal to PHR, especially at rostral levels. Contralateral labeling was

overall sparse but homotopic to ipsilateral labeling and present in layer V. The distribution of contralaterally labeled cells was very sparse in PER, POR, and PaS, whereas comparably more labeled cells were observed in LEC and MEC. Other cases with injection of tracer into mPPC confirmed this labeling pattern. Prominent in all cases was a patch of labeled cells in LEC and MEC close to the rhinal fissure which was consistently found in both hemispheres. Also in all four cases, a few labeled cells were found in the ipsilateral CA1 and subiculum of the hippocampal formation (not shown). Both pyramidal cells and interneurons, as judged by their laminar position (Cappaert et al., 2015), were labeled and they were observed at all dorsoventral levels of subiculum but mainly at intermediate dorsoventral levels of CA1.

A large injection of Fast Blue centered caudally in lPPC but extending into neighboring cortical areas (Fig. 3) yielded results similar to those seen after injection of tracer in mPPC, and retrogradely labeled cells were observed in several parahippocampal areas mainly in deep layers. Rostrally in area 36, labeled cells were seen in all cell layers (Fig. 3a) whereas more caudally labeled cells were located in deep layers and the density of labeled cells tapered off (Fig. 3b, c). In area 35 a few labeled cells were densely packed in layer VI rostrally (Fig. 3a), while sparser labeling was seen in layers V and VI at more caudal levels. In POR, labeled cells were abundant deep in layer V (Fig. 3d-f). No preference for dorsal versus ventral PER or POR could be discerned. Similar to what was seen after injections of tracers centered in mPPC, labeled cells in EC after an injection in lPPC were observed mainly superficially in layer V of LEC and MEC throughout their rostrocaudal extents, with a higher concentration of cells close to the rhinal fissure (Fig. 3a-f). A few labeled cells were found in dorsal PrS as well as PaS (not shown). Dorsal to PHR, labeled cells were observed in temporal cortical areas, particularly at rostral

levels, in addition to visual cortices at the most caudal levels. Rostral to PHR, labeled cells were observed caudally in insular and dorsal piriform cortices surrounding the rhinal fissure. Contralaterally, labeled cells were mainly seen in POR, LEC and MEC, while PER, PrS and PaS were devoid of labeling. In two other cases, Fluorogold was injected into lPPC. These injections were smaller than the one described in detail, resulting in overall sparser, but similarly distributed labeling. Labeled cells were found in deep layers of rostral PER, POR, LEC, MEC and PaS in the hemisphere ipsilateral to the injection, while contralateral labeling was virtually absent. Contrary to mPPC injections, no labeled cells were observed in the hippocampal formation after injection into lPPC. In cases where two different tracers were injected into mPPC and lPPC, labeled cells from the two injections were largely intermingled within PHR and occasionally double labeled cells were observed (not illustrated).

*Injections in V2M*

The borders of PPC with secondary visual areas V2M and V2L are quite difficult to unequivocally establish in the rat brain. Although we have established criteria to delineate these areas from each other (Olsen and Witter, 2016), we wanted to assure that we did not miss out on PPC connections, or erroneously ascribe labeling to PPC injections while that should actually be a component of the connectivity patterns of V2. We therefore included available retrograde tracer injections in V2M as well as anterograde tracer injections (described below) in V2M and V2L. An injection of Fast Blue in V2M (Fig. 4) yielded retrogradely labeled cells in several of the parahippocampal areas. Rostrally in PER, the density of labeled cells was high in deep layers of both areas 36 and 35 (Fig. 4a), but quickly tapered off more caudally (Fig. 4b, c). Labeled

cells were also observed in superficial layers (Fig. 4a, b). In POR, densely packed labeled cells were seen in deep layers (Fig. 4e, f), however, at the caudal pole a few cells were labeled in superficial layers as well (Fig. 4f). Labeled cells in EC were sparsely distributed in both the medial and lateral divisions, and were mainly found superficially in layer V close to the rhinal fissure (Fig. 4a-e), similar to the labeling seen in PPC cases described above. Only a few labeled cells were observed in deep layers of dorsal PrS (not shown) and PaS (Fig. 4e). In areas adjacent to PHR, sparse labeling was seen in caudal insular, dorsal piriform, temporal and visual cortices. Contralaterally, labeled cells were sparsely present in rostral PER as well as in LEC, POR, and MEC. In three other cases, tracer was injected into V2M. One case had an injection of Fluorogold placed more rostrally, and the labeling pattern was similar to the described case. In two cases, the injection sites were placed slightly more medially and extended less along the rostrocaudal axis than the described case. Both cases had comparably fewer labeled cells in the PHR that however were distributed similar to the described case.

Anterograde tracing of projections from dorsal association cortices to PHR

We analyzed 30 injections of anterograde tracers in the parietal and occipital domains of the cortex, of which 22 were in PPC (seven in mPPC, nine in lPPC, six in PtP), seven in V2M, and one in V2L. In general, most of the anterograde labeling was found ipsilaterally with the highest density of labeled fibers in superficial layers of the dorsal PrS as well as deep layers of the caudal pole of the cortex.

*Injections in PPC*

After an injection of PHA-L rostrally in mPPC (Fig. 5), a low number of labeled fibers was found in layers I, III and VI rostrally in area 36 (Fig. 5a, b). No labeling was seen caudally in area 36 (Fig. 5c, d), nor in area 35 (Fig. 5a-d). Labeled fibers were also observed in temporal cortex dorsal to PER, particularly at rostral levels. At caudal levels of the brain, labeled fibers extended from the white matter and reached the deep layers of POR and EC, as well as PaS (Fig. 5e). Only a few labeled fibers were observed more superficially in these areas (Fig. 5e). At rostral levels of PrS, labeled fibers were densely distributed in layer I and III of the dorsal portion (Fig. 5g, h), with a few fibers in layer VI. The density of labeling in PrS quickly tapered off at more caudal levels (Fig. 5i). No labeled fibers were observed in the contralateral PrS, PER, POR or EC. A few fibers were found in layer I of PaS contralaterally, running parallel to the pial surface (not shown). The remaining anterograde tracer injections in mPPC confirmed this pattern of labeling. Labeled fibers were consistently found in layers I and III of dorsal PrS, while the density of labeling in PER and caudal PHR was generally weak and varied between cases.

An injection of PHA-L in lPPC (Fig. 6) resulted in sparse labeling primarily rostrally in PER, with slightly more labeled fibers in area 35 than in area 36 (Fig. 6a). Labeling was stronger more rostrally in the fundus of the rhinal fissure, i.e., in insular cortex (not shown), whereas caudal sections through PER did not contain labeled fibers (Fig. 6b, c). Similar to what was seen after anterograde tracer injections in mPPC, at caudal levels a moderately dense plexus of labeled fibers was observed extending from the white matter into deep layers of POR, EC, PaS, and PrS (Fig. 6e). At the most caudal levels of the cortex, some fibers traveled along the POR/EC border and upon reaching layer I of MEC turned ventrally and extended for quite a distance parallel to the pial surface (Fig. 6e, f). At these levels, labeled fibers were also observed in layer I of PaS

(Fig. 6f). Aside from the sparse labeling in layer VI of caudal PrS, labeling in PrS was focused dorsally and rostrally in layers I and III (Fig. 6g, h). Contralaterally, a few labeled fibers were found in rostral PER and PrS (not shown). Other injections in lPPC showed comparable patterns of labeling in PHR. Similar to what was seen after injections of anterograde tracers in mPPC, labeling was consistently seen in layers I and III of dorsal PrS, while the density of labeling in PER and caudal PHR varied between cases.

Following an injection of PHA-L into area PtP (Fig. 7), sparse labeling was observed mainly rostrally in PER (Fig. 7a), which continued more rostrally through the fundus of the rhinal fissure and grew stronger in the insular cortex where a dense plexus of labeled fibers was seen in layers 1, 3 and 5 (not shown). In areas 35 and 36, labeled fibers were found mainly in layers I and III, but also in layer VI of the rostral portion (Fig. 7a, b). Similar to the cases described above, PER labeling quickly tapered off at more caudal levels, but a few labeled fibers persisted in layer I of area 35 on the border with LEC (Fig. 7c). This pattern continued even more caudally, as PER was replaced with POR (Fig. 7d). At this and more caudal levels, fibers were observed to extend from the white matter, reaching the deep layers of POR and following the border with EC to terminate in layers I, III and V of LEC and layer I and III of MEC (Fig. 7e, f). The labeled fibers on the POR/EC border were present also at more caudal levels to that in Fig. 7f, extending to the pole of the hemisphere (not shown). In addition, a dense patch of labeled fibers was seen in layer I of PaS at caudal levels (Fig. 7e, f). The injection in PtP also gave rise to dense labeling in PrS (Fig. 7g-i). As described previously for mPPC and lPPC cases, in the PtP case the labeling was focused in layers I and III dorsally and rostrally in PrS, tapering off at more caudal and ventral levels. Contralaterally, a few labeled fibers were seen in layer I at the border

between area 35 and LEC. Caudally in the contralateral hemisphere fibers were found extending from the white matter along the POR/EC border, reaching layer I at the caudal pole of the cortex. Other injections in PtP showed comparable patterns of labeling in PHR with labeling in dorsal PrS layers I and III being consistent, whereas labeling in caudal PHR varied between cases.

*Injections in V2*

An injection of PHA-L into V2M (Fig. 8) resulted in sparse labeling rostrally in PER areas 36 and 35 (Fig. 8a). Labeled fibers were concentrated in layer V/VI especially in area 35, although some reached layers I and III of both areas. Labeling was also seen deep to the rhinal fissure at more rostral levels, in insular cortex, but abruptly disappeared in PER at more caudal levels (Fig. 8b, c). More caudally, fibers reached layer VI of POR and EC as well as PaS (Fig. 8e). In the latter two areas, fibers were also observed in layer V, and in PaS some reached layer I (Fig. 8e). At very caudal levels, labeled fibers also reached layer I of POR and MEC (Fig. 8f). Labeling in PrS was shifted slightly more caudal after injection of tracer into V2M compared to what was observed following injections in PPC. Similar to injections in PPC, labeling was densest in layers I and III, but there were also several labeled fibers in layer VI (Fig. 8g-i). Although the labeling was strongest dorsally in PrS, a number of labeled fibers extended ventrally through layers I and III, parallel to the pial surface, reaching the border with PaS (Fig. 8h, i). Contralaterally, a few fibers were found rostrally in PER. Other injections in V2M resulted in comparable patterns of anterograde labeling in the PHR. Similar to injections of anterograde tracer in PPC, tracer injections in V2M consistently yielded labeling in layers I and III of dorsal PrS. Different from what was seen after injections of tracers in PPC, some V2M cases had labeled fibers running

through superficial layers of ventral PrS as described above. In addition, while the POR labeling in PPC cases was largely confined to layer VI at caudal levels, some V2M cases had notably higher density of labeled fibers in more superficial layers of POR. Only one anterograde tracer injection into V2L was available (not illustrated). This BDA injection resulted in a labeling pattern similar to that seen in cases of tracer injections into V2M.

*Lack of strong direct projections from PPC to MEC*

The anterograde data indicated that projections from PPC, and other dorsal association cortices, to MEC are sparse. In view of the potential functional relevance of interactions between PPC and MEC (Whitlock et al., 2008; Whitlock, 2014; Wilber et al., 2014), we decided to corroborate this observation with the use of sensitive transsynaptic viral tracing with rabies virus. We analyzed seven injections of a genetically modified rabies virus in MEC. Disynaptic transport of the virus was apparent after four days survival time, at which point cases displayed labeled cells in the contralateral hippocampus that became more numerous with increased survival time (Ohara et al., 2009). In one animal, the virus injection involved superficial layers of dorsal MEC, and allowing time for only monosynaptic transport (two days), just a few labeled cells were seen in PPC (Fig. 9a). In another animal, the injection of virus was also centered in superficial layers of MEC and was placed slightly more laterally than the first case. This animal survived for five days post infection to allow for disynaptic transport and in this case, some labeled cells were found in layer 5 medially in PPC, but labeled cells were also seen in layers 3 and 6 at more lateral levels (Fig. 9b). In both cases, relatively higher numbers of labeled cells were observed in the caudally adjacent visual areas compared to PPC. These observations thus corroborate the

finding that PPC only sparsely projects to MEC. It is noteworthy that the retrograde rabies tracing showed substantial labeling in dorsal PrS, caudal PaS, POR, and RSC already after two days (not shown), corroborating that these areas provide major inputs to MEC (Caballero-Bleda and Witter, 1993; 1994; van Haeften et al., 1997; Burwell and Amaral, 1998a; b; Jones and Witter, 2007; Canto et al., 2012; Kononenko and Witter, 2012; Czajkowski et al., 2013; Koganezawa et al., 2015; Sugar and Witter, 2016). In view of the observed labeling in all of these areas following anterograde tracer injections in PPC, we infer that PPC might influence MEC most likely by way of these four areas. We therefore decided to use the available experimental dataset to also analyze the connectivity between PPC and RSC.

Connections with RSC

Injections of retrograde and anterograde tracers in parietal and secondary visual cortices generally yielded moderate labeling in ipsilateral area 30, the dysgranular portion of RSC, while less labeling was seen in area 29. Overall, PPC and V2 areas projected to a more restricted portion of RSC than they received input from. In most cases we observed labeling also in contralateral rostral RSC, which was sparse but consistently homotopic to the strongest ipsilateral labeling and confined to area 30.

*Injections in PPC*

A representative injection of Fast Blue centered rostrally in mPPC (Fig. 10, inset 1, panels a-f) resulted in retrogradely labeled cells that were situated mainly in the rostral half of area 30. The

majority of labeled cells was seen in layer V, but some labeled cells were also observed in layers II/III. At the level of the splenium of the corpus callosum, labeled cells were seen in all layers (Fig. 10d). Also at this level, labeled cells were observed in superficial and deep layers of area 29, close to the border with area 30, but little labeling was seen at more caudal levels. In adjacent cortices, strong labeling was seen in the caudal tail of M2 (Fig. 10a, b). More caudally, a substantial number of labeled cells was situated in all layers of V2M along the rostrocaudal axis (Fig. 10c-f). Other cases with injections of retrograde tracers in mPPC largely confirmed this labeling pattern. In one case, with the injection site located more caudally in the cortex, impinging on V2M, labeled cells were observed throughout the rostrocaudal extent of area 30 and extended through most of area 29 along the dorsoventral and rostrocaudal axes.

An anterograde PHA-L injection in mPPC (Fig. 10, inset 2, panels g-l) resulted in labeled fibers which extended from the white matter to the pia, terminating densely in layers I and III of area 30 (Fig. 10g, h, l). These fibers protruded ventrally, eventually crossing the border to area 29, terminating sparsely in superficial layers. The majority of labeling was found at rostral levels, although a sparse plexus was also observed caudally (Fig. 10l). We further noted dense labeling in the caudal portion of M2 (Fig. 10g). As M2 was replaced by V2M, the labeling disappeared (Fig. 10h, i), however, labeled fibers were visible more caudally in V2M (Fig. 10j-l). Other cases of anterograde tracer injections in mPPC confirmed this pattern, showing a moderately dense cluster of labeled fibers rostrally in area 30 and sparse labeling in area 29. In three cases that had injection sites located more caudally in mPPC, labeled fibers in area 30 extended continuously to levels caudal to the splenium.

An injection of the retrograde tracer Fluorogold in lPPC (Fig. 11, inset 1, panels a-f) resulted in retrogradely labeled cells in area 30, the highest concentration of labeled cells was found at rostral levels. Similar to the above described injection in mPPC, labeled cells were mainly situated in layer V and only a few labeled cells were observed in superficial layers (Fig. 11a-e). Only one labeled cell was observed in area 29. We additionally observed labeled neurons in caudal M2 as well as V2M, mainly in layers 2/3 and 5 (Fig. 11a-f).

In a representative case, BDA was injected in lPPC (Fig. 11, inset 2, panels g-l) and a sparse plexus of anterogradely labeled fibers was observed in RSC area 30 (Fig. 11g), extending from the white matter and terminating mainly in layers I, superficial V and VI. The labeling was restricted to only the most rostral sections (Fig. 11g, h) and no labeled fibers were observed in area 29. Lateral to RSC, sparse labeling was seen mainly in deep layers in the caudal extreme of M2 (Fig. 11g, h), and in layer 6 of the lateral portion of V2M (Fig. 11i, j). The weak V2M labeling was shifted more rostrally than in case of injections into mPPC. All other cases with injections of anterograde tracer in lPPC contained a sparse to moderately dense plexus of labeled fibers in area 30. In some cases, labeled fibers were observed in area 29, but the density of labeled fibers in area 29 was always much weaker than in area 30.

Regarding PtP, we unfortunately did not obtain an injection of a retrograde tracer so we only had successful injections of anterograde tracers in PtP. Due to the limited mediolateral extent of this parietal area, tracer injections extended into either the medially adjacent V2L or the laterally

adjacent S1. In a representative case, having an injection impinging on V2L (Fig. 12, inset 1, panels a-f), a sparse plexus of PHA-L labeled fibers was seen in area 30 at rostral levels (Fig. 12a, b). The fibers terminated mainly in layer I but individual fibers were seen in other layers as well. Notable labeling was also seen rostrally in area 29, mainly in layers I and VI (Fig. 12a, b). On the other hand, the laterally adjacent M2 and V2M contained only scattered labeled fibers (Fig. 12a-f). Two other injections in PtP impinged on V2L as well (not shown), and yielded similar results. In contrast, three injections were placed more laterally and extended into S1 (not shown). One of these contained sparse labeling in area 30, whereas two others contained only a few labeled fibers in RSC. It is therefore possible that the observed labeling in areas 30 and 29 in the described case was a result of the tracer injection extending into V2L which projects to RSC (see below).

*Injections in V2*

A representative injection of Fast Blue in V2M (Fig. 13, inset 1, panels a-f) yielded similar results as the above described injections in PPC subdivisions, as the majority of retrogradely labeled cells were located in layer V of area 30, with fewer labeled cells situated in superficial layers (Fig. 13a-f). However, the rostrocaudal location of the labeled cells appeared to be shifted to a more caudal level than in the PPC cases, since there were few labeled cells at the most rostral level (Fig. 13a) and labeled cells were observed at levels several millimeters caudal to the splenium of the corpus callosum (Fig. 13d-f). Similarly, labeled cells in area 29 were observed across a wide rostrocaudal extent (Fig. 13b-e). Clusters of labeled cells were also observed in layers 2/3 and 5 of V2M at several rostrocaudal levels (Fig. 13c, e, f), representing intrinsic

secondary visual connections, whereas the caudal portion of M2 was devoid of labeling. Other injections of retrograde tracer in V2M yielded similar results.

Injections of anterograde tracers in V2M resulted in moderate labeling in RSC, which was shifted slightly caudal to the labeling seen in case of injections in PPC. In a representative case, PHA-L was injected rostrally in V2M (Fig. 13, inset 2, panels g-l). Only scattered PHA-L labeled fibers were found at the most rostral levels of area 30 (Fig. 13g), but more caudally a moderate plexus of labeled fibers was seen (Fig. 13h, i) terminating mainly in layers I and VI. The labeling tapered off at the level of the splenium of the corpus callosum (Fig. 13j) and disappeared at more caudal levels (Fig. 13k-l). Fibers extended ventrally, reaching area 29 (Fig. 13h-j). Very few labeled fibers were observed in caudal M2 (Fig. 13g), whereas intrinsic projections to visual areas were notable especially at mid-rostrocaudal levels of V2M (Fig. 13j). All other cases with injections of anterograde tracer in V2M yielded a moderate to dense plexus of labeled fibers in area 30 that in most cases extended continuously from rostral levels to levels caudal to the splenium. Labeled fibers were also consistently found in area 29, but the density of this labeling varied between cases. A case of BDA injection in V2L (not shown) resulted in similar labeling as tracer injections in V2M, with labeled fibers distributed mainly in layer I and VI of area 30.

**Discussion**

The PPC and V2 and their respective subdivisions are cytoarchitectonically distinct areas with different thalamic connections (Olsen and Witter, 2016). It is therefore noteworthy that all areas

appear to be reciprocally connected to all divisions of the PHR and to RSC area 30, albeit with subtle topographical differences (Fig. 14). The connections with PrS and PaS are biased towards PPC and V2 projecting to both areas, while the return projections seem to be much weaker, or almost absent. Overall, projections from PPC and V2 to EC seem to be among the weakest of all, while return projections originate mainly from the most dorsolateral and caudal domains of EC. We further noted that connections of PPC and V2 with PER are preferentially with a rostral domain and in some instances extending beyond what we consider the rostral border of PER, thus invading the adjacent insular cortex. We reported the labeling pattern observed from approximately 4 mm caudal to bregma. At that level, claustral cells were no longer observed, and the trilaminar appearance of the insular cortex was completely disintegrated. More rostral labeling coincided with a more laminated structure of the cortex and the appearance of a few claustral cells, presented as a thin sheet deep to the cortex. These features to us indicate that this is insular cortex. However, the exact rostrocaudal level at which the insular cortex disappears and PER appears in the rat brain is debated (Burwell, 2001; Paxinos and Watson, 2007; Kjønigsen et al., 2011; Boccara et al., 2015).

## Connections of dorsal association cortices with parahippocampal areas

### *Parahippocampal input to dorsal association cortices*

Both PPC and V2 appear to receive input predominantly from deep layers of PER, POR, and EC, while PrS and PaS seem to originate only sparse projections to these dorsal association cortices. These results largely confirm findings from previous studies (Miller and Vogt, 1984; Reep et al., 1994; Agster and Burwell, 2009) but in the present study we add details on the topographical

distributions of these projections. Our data show that mPPC, lPPC and V2M all receive inputs that originate mainly in rostral PER as well as POR. Moderate to dense projections to PPC and V2 from POR have previously been described in an extensive study of PHR efferents using anterograde tracers (Agster and Burwell, 2009). These authors also reported sparse input from area 35 and moderate input from rostral area 36 to mPPC and lPPC. Contrary to our results, however, they concluded that caudal area 36 provides the main PER input to V2M whereas our retrograde data indicate only a weak caudal PER input to V2M. This apparent discrepancy is most likely caused by limitations of anterograde tracing and it is plausible that the caudal PER injections of Agster and colleagues (2009) also involved rostral POR which, as mentioned above, originates moderate projections to PPC and V2. The origin of PER and POR projections to dorsal association areas in deep layers is in line with previous studies which in addition have shown that they terminate in superficial layers (Miller and Vogt, 1984; Reep et al., 1994; Agster and Burwell, 2009), although POR projections to visual cortices terminate across superficial and deep layers (Agster and Burwell, 2009).

Our data corroborate several studies employing anterograde and retrograde tracers in showing that EC provides only sparse input to dorsal association areas, originating in EC layer V (Swanson and Kohler, 1986; Insausti et al., 1997; Agster and Burwell, 2009; Wilber et al., 2015). All reports emphasize that the majority of entorhinal projections arise from a portion of both LEC and MEC close to the rhinal fissure, i.e., the dorsolateral strip of EC that is preferentially connected with the septal hippocampus (Witter et al., 1989; Dolorfo and Amaral, 1998). Similar to PER and POR, EC projections to PPC and V2M terminate in superficial layers (Agster and Burwell, 2009).

Only a few labeled cells were observed in deep layers of PrS and PaS after injections of retrograde tracers in dorsal association areas. Such input has previously been described for V2M after injections of retrograde tracers in this area (Vogt and Miller, 1983), while two studies of PrS and PaS efferents employing anterograde tracers did not describe projections to dorsal association areas (van Groen and Wyss, 1990a; c). We therefore conclude that PrS and PaS provide only minimal input to mPPC, lPPC and V2M.

Previously, it has been shown that CA1 of the hippocampal formation in rat originates projections to widespread areas of the cortex, including a very sparse projection that targets layer 6 of PPC, and that this projection originates in the ventral two thirds of CA1 (Cenquizca and Swanson, 2007). Our data confirms and extends this finding, showing that an additional sparse projection arises from all dorsoventral levels of subiculum, moreover, hippocampal projections appear to target only mPPC.

The projections from RSC to mPPC, lPPC and V2M reported here have previously been described as well (van Groen and Wyss, 1992; Reep et al., 1994; Wilber et al., 2015). Our findings suggest that the majority of projections arise from the rostral half of RSC, which is in contrast to a report that injections of anterograde tracers into caudal but not rostral RSC area 30 produced a substantial amount of labeled fibers in V2M (van Groen and Wyss, 1992). We did not see a significant difference in RSC input to mPPC versus lPPC, which is in contrast to a study in which it was reported that RSC projects stronger to mPPC than to lPPC (Wilber et al.,

2015). Our results further showed that the RSC projections to dorsal association areas originated mainly in layer V and less in layer III, supplementing previous descriptions of these projections terminating in layers 1 and 3-5 of V2M (van Groen and Wyss, 1992). The laminar termination pattern of RSC projections to PPC has to our knowledge not yet been described, but a review of existing material in our lab (injections in area 30 described in Jones and Witter, 2007) revealed a sparse projection preferentially to layer 1, although fibers were occasionally observed in other layers particularly in mPPC.

*Projections from dorsal association cortices to the parahippocampal region*

Projections from PPC and visual association cortices appear to target similar portions of the PHR, in that projections from all areas targeted rostral PER, POR, caudal EC, caudal PaS and rostrodorsal PrS, however, subtle topographies could be discerned. For instance, sparse PPC projections to rostral PER preferentially targeted area 36, whereas V2 projections were denser in area 35. PPC input to rostral area 36 was previously described in an extensive study of PHR afferents employing retrograde tracer injections in the region, but contrary to our results these authors found that V2 projections targeted only the most caudal extreme of area 36 (Burwell and Amaral, 1998a). Considering the lack of labeled V2 projections in caudal area 36 in our hands, as well as the shared observation about projections from V2M as well as PPC to POR (present study; Miller and Vogt, 1984; Burwell and Amaral, 1998a), we find it plausible that the retrograde tracer injection in caudal area 36 in the latter study involved POR as well as caudal PER. Our data additionally show that the majority of projections from PPC subdivisions and V2M target deep layers of caudal POR. We further conclude, in line with a previous study

(Burwell and Amaral, 1998a), that projections from V2 to POR are stronger than those from PPC since they terminate not only in deep layers, as is the case for PPC projections, but also in superficial layers.

Our results also indicate that PPC and V2 project to EC, preferentially to deep layers of the most caudal portion close to the rhinal fissure. These observations are largely in line with a previous study describing sparse input from dorsal association areas after injections of retrograde tracers in caudal EC, with each of the V2 subdivisions providing a similar proportion of input as the PPC, and a higher proportion of input to MEC than to LEC (Burwell and Amaral, 1998a). Different from this, our results suggest that fibers from all dorsal association areas target caudal LEC and MEC equally. In a study in which injections of tritiated amino acids were placed in visual cortices, projections to EC were not reported (Miller and Vogt, 1984), likely because these tracers are less sensitive than the ones we have employed. Projections from PPC to PER, POR and EC have been found to originate in layers 2, superficial 5, and 6, while projections from V2 originated from layers 2 and 6 (Burwell and Amaral, 1998a).

To our knowledge, ours is the first account of direct PPC projections to PrS and PaS in the rat, whereas projections from V2 to dorsal PrS have previously been described and shown to originate in layer 5 (Vogt and Miller, 1983; van Groen and Wyss, 1990c). Our results corroborate that projections from V2M mainly terminate in layers I and III of dorsal PrS, and that these extend into ventral levels of PrS (Vogt and Miller, 1983). Our findings suggest that PPC projections to PrS are confined to the dorsal portion and are shifted slightly rostral

compared with V2 projections. Inputs from PPC or V2 were not described after injections of retrograde tracers in PaS (van Groen and Wyss, 1990a), possibly because, according to our data, these projections target only a small, caudal portion of PaS.

In line with previous studies (van Groen and Wyss, 1992; Wilber et al., 2015), we found that PPC and V2 also project to RSC. We report that these projections mainly target rostral parts of area 30, and distribute to deep layers as well as layers I and III. The superficial termination in RSC of V2M projections was previously described in a study where they were also found to originate in deep layers (van Groen and Wyss, 1992). The same authors further reported that injections of retrograde tracers in caudal RSC resulted in higher numbers of labeled cells in V2M than injections in rostral RSC (van Groen and Wyss, 1992), in contrast to our findings that PPC and V2 preferentially target rostral RSC. The preferred projection to area 30 over area 29 substantiates the notion that area 30 has stronger connections with cortical areas outside the PHR and subicular complex than area 29 (Wyss and Van Groen, 1992).

Comparative considerations

Different from the rat, the monkey PPC comprises an area 5 in addition to area 7. However, area 5 is closely associated with somatosensory areas and does not connect with the PHR (Seltzer and Pandya, 1976; 1984; Cavada and Goldman-Rakic, 1989a; Suzuki and Amaral, 1994; Muñoz and Insausti, 2005). For area 7, connections with the PHR have mainly been described for the caudomedial area 7a of the inferior parietal lobule, whereas the more rostrolateral area 7b appears not to be connected with PHR (Seltzer and Pandya, 1976; 1984; Stanton et al., 1977;

Cavada and Goldman-Rakic, 1989a). Studies of areas embedded in the intraparietal sulcus have yielded conflicting results pertaining to connections with PHR (Cavada and Goldman-Rakic, 1989a; Andersen et al., 1990; Suzuki and Amaral, 1994; Lewis and Van Essen, 2000).

Weak projections to PER from area 7 have been observed in the monkey (Seltzer and Pandya, 1984; Suzuki and Amaral, 1994) although reciprocal projections were not found (Lavenex et al., 2002). Confined bidirectional connections with EC have also been described (Muñoz and Insausti, 2005; Insausti and Amaral, 2008). This is consistent with our findings of weak connections of rat PPC with PER and EC. In contrast, a large body of literature has described a strong, bilateral and reciprocal connection of monkey area 7a with the parahippocampal cortex, homolog to POR in the rat (Pandya and Vignolo, 1969; Seltzer and Pandya, 1976; 1984; Stanton et al., 1977; Cavada and Goldman-Rakic, 1989a; Andersen et al., 1990; Suzuki and Amaral, 1994; Lavenex et al., 2002; Muñoz and Insausti, 2005). However, while area 7a of the monkey PPC is just connected with subdivision TF of the parahippocampal cortex, our data suggests that all subdivisions of rat PPC are reciprocally connected with the whole POR. Similarly, a projection mainly arising from monkey area 7a to PrS has been described that targets layers I and III of the caudal PrS and is reciprocated by sparse projections from deep layers of this area (Seltzer and Van Hoesen, 1979; Seltzer and Pandya, 1984; Cavada and Goldman-Rakic, 1989a; Andersen et al., 1990; Ding et al., 2000; Insausti and Muñoz, 2001). Our findings in the rat corroborate the sparse projection from PrS to PPC as well as the denser reciprocal projections from PPC to dorsal PrS terminating in layers I and III, but contrasting findings in the monkey, our data suggest that rat PrS receives input from all subdivisions of PPC.

Two studies reported very fine fibers originating in monkey area 7 that terminated in CA1 of the hippocampal formation (Rockland and Van Hoesen, 1999; Ding et al., 2000), while projections from CA1 or subiculum were not found after injections of retrograde tracers in PPC (Insausti and Muñoz, 2001). In contrast to this, in our hands, such injections in the rat mPPC yielded a few labeled cells in CA1 and subiculum of the hippocampus, whereas injections of anterograde tracers in PPC did not result in labeled fibers in the hippocampus. We do note that the reported labeled fibers in monkey CA1 were very thin and only observed at high magnification after large injections of tracer (Rockland and Van Hoesen, 1999; Ding et al., 2000), similarly, our material showed that PPC-projecting cells in CA1 and subiculum in the rat were scarce, hence the sparsity of the reciprocal PPC-hippocampus connections suggests they could easily be missed if injections were too small.

In sum, our findings in rat show that connections between PPC and PER, EC, and PrS are largely comparable to those observed in monkeys. In contrast, the connection of rat PPC with POR lacks the precise topographical organization that is seen in monkeys where only a subdivision of PPC is connected with a portion of the primate parahippocampal cortex. Previous studies have pointed out that interconnectivity between higher order areas may be less specific in the rat than in monkeys (Burwell and Amaral, 1998a) and that there is a higher degree of segregated information processing in the monkey than in the rat – pointing to a higher level of parallel processing in primates compared to rodents (Lavenex and Amaral, 2000).

A proposed diagram of parietal-parahippocampal interactions.

Results from early behavioral studies indicated that PPC is involved in aspects of spatial navigation, for instance, recording studies found properties of PPC cells that were assumed to be spatially modulated (head direction cells, Chen et al., 1994; forming representations of routes, Nitz, 2006) and lesions of PPC resulted in deficits in tasks testing spatial memory (Kolb and Walkey, 1987; Save and Poucet, 2000b; Rogers and Kesner, 2007). One logical assumption was thus that PPC interacts with the hippocampus or the associated PHR, both of which are heavily involved in such behavior. We however conclude that direct connections between the two cortical domains are limited, substantiating behavioral studies where a double dissociation has been described between their functions (for review, see Kesner, 2009; Save and Poucet, 2009). Our results suggest that interactions between PPC and PHR most likely are mediated through POR and PrS, as well as RSC area 30 (Fig. 14). All three areas likely integrate the signals they convey between PPC and PHR, such that three functionally different pathways may exist, which each uniquely contribute to the complex functional profile of PPC. In the subsequent paragraphs, we summarize the intricate connectional diagram, aiming to derive some functional insight.

POR is reciprocally connected with PPC (Burwell and Amaral, 1998a; Agster and Burwell, 2009), and is also reciprocally connected with MEC (Burwell and Amaral, 1998a; b) providing a major excitatory input to superficial layers of MEC (Koganezawa et al., 2015). Since the sparse PPC projections mainly target layer VI of POR while projections to MEC originate in superficial layers of this area (Burwell and Amaral, 1998b; Koganezawa et al., 2015), it is likely that local POR circuits need to be bypassed but the detailed circuitry within POR remains to be

established. It is worth mentioning that POR receives a larger proportion of input from V2 than from PPC (Burwell and Amaral, 1998a), suggesting that visual areas may have a stronger influence on POR activity than PPC.

With respect to PrS, we conclude that the dorsal portion receives equally dense input from PPC and from secondary visual cortex, the latter corroborating previous findings (Vogt and Miller, 1983; van Groen and Wyss, 1990c). Both inputs show a preferred termination in layers I and III, and overlap partially with layer III-projecting terminals from RSC. Pyramidal neurons in layer III, in turn, constitute the main origin of PrS projections to MEC where they terminate in superficial layers (Caballero-Bleda and Witter, 1993; 1994; van Haeften et al., 1997; Kononenko and Witter, 2012; Agster and Burwell, 2013). It is thus feasible that PPC and V2 inputs might target layer III PrS neurons mediating this input to MEC. However, this proposition and whether RSC, PPC and V2M inputs impinge on the same layer III neurons awaits further testing. Similar to PrS, PaS provides input to superficial layers of MEC targeting hippocampal-projecting cells (van Groen and Wyss, 1990a; Caballero-Bleda and Witter, 1993; 1994), and although projections from PaS and PrS terminate in separate layers, monosynaptic input from both areas is integrated by principal neurons in all layers of MEC (Canto et al., 2012). The precise role of PaS, compared to that of PrS is still poorly understood, although cells relevant to navigation have been described in both areas (Taube et al., 1990a; b; Taube, 1995; Boccara et al., 2015).

RSC is another candidate structure to mediate PPC interactions with the parahippocampal-hippocampal system as has been suggested by others (Save and Poucet, 2000a; Whitlock et al.,

2008; Whitlock, 2014; Wilber et al., 2015), since it has direct projections to MEC (Burwell and Amaral, 1998a; Jones and Witter, 2007; Czajkowski et al., 2013; Sugar and Witter, 2016). However, some observations from our data in combination with previous studies suggest that this may be an inefficient route to the hippocampal-projecting cells of MEC. First, PPC projects preferentially to rostral RSC, while it is the caudal RSC that originates the heaviest input to MEC (Jones and Witter, 2007; Sugar and Witter, 2016). Second, RSC projections mainly terminates in layer V of MEC (Burwell and Amaral, 1998a; Jones and Witter, 2007; Czajkowski et al., 2013; Sugar and Witter, 2016) where the receiving neurons relay to superficial layers (Czajkowski et al., 2013). Thus, even though RSC projects directly to MEC, several relays within RSC and MEC are necessary for information from PPC to reach superficial layers of MEC. On the other hand, the whole rostrocaudal axis of RSC strongly projects to PrS (Jones and Witter, 2007) adding importance to this area as a relay, since it, similar to POR, distribute projections to superficial layers of MEC, likely targeting hippocampal-projecting neurons (Caballero-Bleda and Witter, 1993; 1994; van Haeften et al., 1997; Kononenko and Witter, 2012; Koganezawa et al., 2015) although synaptic contacts are made onto layer V neurons as well (Canto et al., 2012). In sum, PrS remains as the parahippocampal area that provides the most efficient route for PPC projections to reach superficial layers of MEC and ultimately the hippocampal formation.

PrS may integrate information from multiple sensory modalities, head direction, an internal map of the environment as well as the borders surrounding it (Taube et al., 1990a; b; Boccara et al., 2010). Neurons in PPC of rats do not carry a marked spatial code while animals freely forage in an open environment – rather, these neurons predict modes of movement (Whitlock et al., 2012; Wilber et al., 2014), in line with recent studies showing an involvement of rat and mouse PPC in

movement and decision-making (Harvey et al., 2012; Raposo et al., 2014; Erlich et al., 2015; Hanks et al., 2015). While head direction cells in PrS represent the real time head direction signal, they receive anticipatory head directional signals from the anterodorsal thalamic nucleus as well as RSC (Blair and Sharp, 1995; Cho and Sharp, 2001) and PPC projections likely contribute information about planned self-motion and action control (Whitlock et al., 2008; Whitlock, 2014).

Although PrS constitutes the main route for PPC information to influence the hippocampal-parahippocampal system, the sparsity of return projections suggests that PrS does not relay information from PHR to PPC. In contrast, our data indicates that RSC provides significant input to PPC. RSC integrates information about allocentric space from PHR with idiothetic information from the head direction system and possibly from PPC, and cells here map position in external and internal frames of reference (Alexander and Nitz, 2015) that in turn could be used by PPC to guide navigation. Similar to recent findings in rodents that PPC neurons predict movements, early studies of monkeys reported that cells in PPC are active before or during movement of the eyes or limbs (Mountcastle et al., 1975; Robinson et al., 1978). Based on the extensive primate literature, the involvement of PPC in such activities is thought to be enacted in concert with frontal cortical areas since they are heavily interconnected (Cavada and Goldman-Rakic, 1989b; Andersen et al., 1990; Rozzi et al., 2006; Pesaran et al., 2008; Gharbawie et al., 2011; Stepniewska et al., 2011) but although fronto-parietal connections have been described in the rat (Reep et al., 1984, 1987, 1990, 1994, 1996; Kolb and Walkey, 1987; Condé et al., 1995; Hoover and Vertes, 2007; 2011), their exact topographic organization remains to be explored in detail.

## References


Agster KL, Burwell RD. 2009. Cortical efferents of the perirhinal, postrhinal, and entorhinal cortices of the rat. Hippocampus 19(12):28.

Agster KL, Burwell RD. 2013. Hippocampal and subicular efferents and afferents of the perirhinal, postrhinal, and entorhinal cortices of the rat. Behav Brain Res 254:50-64.

Alexander AS, Nitz DA. 2015. Retrosplenial cortex maps the conjunction of internal and external spaces. Nat Neurosci 18(8):1143-1151.

Andersen RA, Asanuma C, Essick G, Siegel RM. 1990. Corticocortical connections of anatomically and physiologically defined subdivisions within the inferior parietal lobule. J Comp Neurol 296(1):65-113.

Blair HT, Sharp PE. 1995. Anticipatory head direction signals in anterior thalamus: evidence for a thalamocortical circuit that integrates angular head motion to compute head direction. J Neurosci 15(9):6260-6270.

Boccara CN, Kjønigsen LJ, Hammer IM, Bjaalie JG, Leergaard TB, Witter MP. 2015. A three-plane architectonic atlas of the rat hippocampal region. Hippocampus 25(7):838-857.

Boccara CN, Sargolini F, Thoresen VH, Solstad T, Witter MP, Moser EI, Moser MB. 2010. Grid cells in pre- and parasubiculum. Nat Neurosci 13(8):987-994.

Burwell RD. 2001. Borders and cytoarchitecture of the perirhinal and postrhinal cortices in the rat. J Comp Neurol 437(1):17-41.

Burwell RD, Amaral DG. 1998a. Cortical afferents of the perirhinal, postrhinal, and entorhinal cortices of the rat. J Comp Neurol 398(2):179-205.

Burwell RD, Amaral DG. 1998b. Perirhinal and postrhinal cortices of the rat: interconnectivity and connections with the entorhinal cortex. J Comp Neurol 391(3):293-321.

Caballero-Bleda M, Witter MP. 1993. Regional and laminar organization of projections from the presubiculum and parasubiculum to the entorhinal cortex: an anterograde tracing study in the rat. J Comp Neurol 328(1):115-129.

Caballero-Bleda M, Witter MP. 1994. Projections from the presubiculum and the parasubiculum to morphologically characterized entorhinal-hippocampal projection neurons in the rat. Exp Brain Res 101(1):93-108.

Canto CB, Koganezawa N, Beed P, Moser EI, Witter MP. 2012. All layers of medial entorhinal cortex receive presubicular and parasubicular inputs. J Neurosci 32(49):17620-17631.

Cappaert NL, Van Strien NM, Witter MP. 2015. Hippocampal Formation. In: Paxinos G, ed. The Rat Nervous System. Fourth ed. p 511-573.

Cavada C, Goldman-Rakic PS. 1989a. Posterior parietal cortex in rhesus monkey: I. Parcellation of areas based on distinctive limbic and sensory corticocortical connections. J Comp Neurol 287(4):393-421.

Cavada C, Goldman-Rakic PS. 1989b. Posterior parietal cortex in rhesus monkey: II. Evidence for segregated corticocortical networks linking sensory and limbic areas with the frontal lobe. J Comp Neurol 287(4):422-445.

Cenquizca LA, Swanson LW. 2007. Spatial organization of direct hippocampal field CA1 axonal projections to the rest of the cerebral cortex. Brain research reviews 56(1):1-26.

Chen LL, Lin LH, Green EJ, Barnes CA, McNaughton BL. 1994. Head-direction cells in the rat posterior cortex. I. Anatomical distribution and behavioral modulation. Exp Brain Res 101(1):8-23.

Cho J, Sharp PE. 2001. Head direction, place, and movement correlates for cells in the rat retrosplenial cortex. Behav Neurosci 115(1):3-25.
Condé F, Maire-Lepoivre E, Audinat E, Crépel F. 1995. Afferent connections of the medial frontal cortex of the rat. II. Cortical and subcortical afferents. J Comp Neurol 352(4):567-593.
Czajkowski R, Sugar J, Zhang SJ, Couey JJ, Ye J, Witter MP. 2013. Superficially Projecting Principal Neurons in Layer V of Medial Entorhinal Cortex in the Rat Receive Excitatory Retrosplenial Input. J Neurosci 33(40):15779-15792.
DiMattia BV, Kesner RP. 1988. Role of the posterior parietal association cortex in the processing of spatial event information. Behav Neurosci 102(3):397-403.
Ding SL, Van Hoesen G, Rockland KS. 2000. Inferior parietal lobule projections to the presubiculum and neighboring ventromedial temporal cortical areas. J Comp Neurol 425(4):510-530.
Dolorfo CL, Amaral DG. 1998. Entorhinal cortex of the rat: topographic organization of the cells of origin of the perforant path projection to the dentate gyrus. J Comp Neurol 398(1):25-48.
Erlich JC, Brunton BW, Duan CA, Hanks TD, Brody CD. 2015. Distinct effects of prefrontal and parietal cortex inactivations on an accumulation of evidence task in the rat. eLife 4:e05457.
Fyhn M, Molden S, Witter MP, Moser EI, Moser MB. 2004. Spatial representation in the entorhinal cortex. Science 305(5688):1258-1264.
Gharbawie OA, Stepniewska I, Kaas JH. 2011. Cortical connections of functional zones in posterior parietal cortex and frontal cortex motor regions in new world monkeys. Cereb Cortex 21(9):1981-2002.
Hafting T, Fyhn M, Molden S, Moser MB, Moser EI. 2005. Microstructure of a spatial map in the entorhinal cortex. Nature 436(7052):801-806.
Hanks TD, Kopec CD, Brunton BW, Duan CA, Erlich JC, Brody CD. 2015. Distinct relationships of parietal and prefrontal cortices to evidence accumulation. Nature 520(7546):220-223.
Harvey CD, Coen P, Tank DW. 2012. Choice-specific sequences in parietal cortex during a virtual-navigation decision task. Nature 484(7392):62-68.
Hoover WB, Vertes RP. 2007. Anatomical analysis of afferent projections to the medial prefrontal cortex in the rat. Brain structure & function 212(2):149-179.
Hoover WB, Vertes RP. 2011. Projections of the medial orbital and ventral orbital cortex in the rat. J Comp Neurol 519(18):3766-3801.
Inoue K, Ohara S, Ichijyo H, Kakei S, Iijima T. 2004. Development of rabies virus vectors for neuron-specific and transsynaptic delivery of a foreign gene (Abstract). Soc Neurosci Abstr 30(124.12).
Insausti R, Amaral DG. 2008. Entorhinal cortex of the monkey: IV. Topographical and laminar organization of cortical afferents. J Comp Neurol 509(6):608-641.
Insausti R, Herrero MT, Witter MP. 1997. Entorhinal cortex of the rat: cytoarchitectonic subdivisions and the origin and distribution of cortical efferents. Hippocampus 7(2):146-183.
Insausti R, Muñoz M. 2001. Cortical projections of the non-entorhinal hippocampal formation in the cynomolgus monkey (Macaca fascicularis). Eur J Neurosci 14(3):435-451.
Jarrard LE, Davidson TL, Bowring B. 2004. Functional differentiation within the medial temporal lobe in the rat. Hippocampus 14(4):434-449.
Jones BF, Witter MP. 2007. Cingulate cortex projections to the parahippocampal region and hippocampal formation in the rat. Hippocampus 17(10):957-976.
Kesner RP. 2009. The posterior parietal cortex and long-term memory representation of spatial information. Neurobiol Learn Mem 91(2):197-206.
Kjønigsen LJ, Leergaard TB, Witter MP, Bjaalie JG. 2011. Digital atlas of anatomical subdivisions and boundaries of the rat hippocampal region. Frontiers in neuroinformatics 5(Article 2).
Koganezawa N, Gisetstad R, Husby E, Doan TP, Witter MP. 2015. Excitatory Postrhinal Projections to Principal Cells in the Medial Entorhinal Cortex. J Neurosci 35(48):15860-15874.

Kolb B, Sutherland RJ, Whishaw IQ. 1983. A comparison of the contributions of the frontal and parietal association cortex to spatial localization in rats. Behav Neurosci 97(1):13-27.
Kolb B, Walkey J. 1987. Behavioural and anatomical studies of the posterior parietal cortex in the rat. Behav Brain Res 23(2):127-145.
Kononenko NL, Witter MP. 2012. Presubiculum layer III conveys retrosplenial input to the medial entorhinal cortex. Hippocampus 22(4):881-895.
Kropff E, Carmichael JE, Moser MB, Moser EI. 2015. Speed cells in the medial entorhinal cortex. Nature 523(7561):419-424.
Lavenex P, Amaral DG. 2000. Hippocampal-neocortical interaction: a hierarchy of associativity. Hippocampus 10(4):420-430.
Lavenex P, Suzuki WA, Amaral DG. 2002. Perirhinal and parahippocampal cortices of the macaque monkey: projections to the neocortex. J Comp Neurol 447(4):394-420.
Lewis JW, Van Essen DC. 2000. Corticocortical connections of visual, sensorimotor, and multimodal processing areas in the parietal lobe of the macaque monkey. J Comp Neurol 428(1):112-137.
Miller MW, Vogt BA. 1984. Direct connections of rat visual cortex with sensory, motor, and association cortices. J Comp Neurol 226(2):184-202.
Morris RG, Garrud P, Rawlins JN, O'Keefe J. 1982. Place navigation impaired in rats with hippocampal lesions. Nature 297(5868):681-683.
Mountcastle VB, Lynch JC, Georgopoulos A, Sakata H, Acuna C. 1975. Posterior parietal association cortex of the monkey: command functions for operations within extrapersonal space. J Neurophysiol 38(4):871-908.
Muñoz M, Insausti R. 2005. Cortical efferents of the entorhinal cortex and the adjacent parahippocampal region in the monkey (Macaca fascicularis). Eur J Neurosci 22(6):1368-1388.
Nitz DA. 2006. Tracking route progression in the posterior parietal cortex. Neuron 49(5):747-756.
Nitz DA. 2012. Spaces within spaces: rat parietal cortex neurons register position across three reference frames. Nat Neurosci 15(10):1365-1367.
O'Keefe J, Dostrovsky J. 1971. The hippocampus as a spatial map. Preliminary evidence from unit activity in the freely-moving rat. Brain Res 34(1):171-175.
Ohara S, Inoue K, Yamada M, Yamawaki T, Koganezawa N, Tsutsui K, Witter MP, Iijima T. 2009. Dual transneuronal tracing in the rat entorhinal-hippocampal circuit by intracerebral injection of recombinant rabies virus vectors. Front Neuroanat 3(Article 1).
Olsen GM, Witter MP. 2016. Posterior parietal cortex of the rat: Architectural delineation and thalamic differentiation. J Comp Neurol 524(18):3774-3809.
Pandya DN, Vignolo LA. 1969. Interhemispheric projections of the parietal lobe in the rhesus monkey. Brain Res 15(1):49-65.
Paxinos G, Watson C. 2007. The rat brain in stereotaxic coordinates. Amsterdam: Elsevier. 462 p.
Pesaran B, Nelson MJ, Andersen RA. 2008. Free choice activates a decision circuit between frontal and parietal cortex. Nature 453(7193):406-409.
Raposo D, Kaufman MT, Churchland AK. 2014. A category-free neural population supports evolving demands during decision-making. Nat Neurosci 17(12):1784-1792.
Reep RL, Chandler HC, King V, Corwin JV. 1994. Rat posterior parietal cortex: topography of corticocortical and thalamic connections. Exp Brain Res 100(1):67-84.
Reep RL, Corwin JV, Hashimoto A, Watson RT. 1984. Afferent connections of medial precentral cortex in the rat. Neurosci Lett 44(3):247-252.
Reep RL, Corwin JV, Hashimoto A, Watson RT. 1987. Efferent connections of the rostral portion of medial agranular cortex in rats. Brain Res Bull 19(2):203-221.
Reep RL, Corwin JV, King V. 1996. Neuronal connections of orbital cortex in rats: topography of cortical and thalamic afferents. Exp Brain Res 111(2):215-232.

Reep RL, Goodwin GS, Corwin JV. 1990. Topographic organization in the corticortical connections of medial agranular cortex in rats. J Comp Neurol 294(2):262-280.
Robinson DL, Goldberg ME, Stanton GB. 1978. Parietal association cortex in the primate: sensory mechanisms and behavioral modulations. J Neurophysiol 41(4):910-932.
Rockland KS, Van Hoesen GW. 1999. Some temporal and parietal cortical connections converge in CA1 of the primate hippocampus. Cereb Cortex 9(3):232-237.
Rogers JL, Kesner RP. 2007. Hippocampal-parietal cortex interactions: evidence from a disconnection study in the rat. Behav Brain Res 179(1):19-27.
Rozzi S, Calzavara R, Belmalih A, Borra E, Gregoriou GG, Matelli M, Luppino G. 2006. Cortical connections of the inferior parietal cortical convexity of the macaque monkey. Cereb Cortex 16(10):1389-1417.
Sargolini F, Fyhn M, Hafting T, McNaughton BL, Witter MP, Moser MB, Moser EI. 2006. Conjunctive representation of position, direction, and velocity in entorhinal cortex. Science 312(5774):758-762.
Save E, Poucet B. 2000a. Hippocampal-parietal cortical interactions in spatial cognition. Hippocampus 10(4):491-499.
Save E, Poucet B. 2000b. Involvement of the hippocampus and associative parietal cortex in the use of proximal and distal landmarks for navigation. Behav Brain Res 109(2):195-206.
Save E, Poucet B. 2009. Role of the parietal cortex in long-term representation of spatial information in the rat. Neurobiol Learn Mem 91(2):172-178.
Seltzer B, Pandya DN. 1976. Some cortical projections to the parahippocampal area in the rhesus monkey. Exp Neurol 50(1):146-160.
Seltzer B, Pandya DN. 1984. Further observations on parieto-temporal connections in the rhesus monkey. Exp Brain Res 55(2):301-312.
Seltzer B, Van Hoesen GW. 1979. A direct inferior parietal lobule projection to the presubiculum in the rhesus monkey. Brain Res 179(1):157-161.
Solstad T, Boccara CN, Kropff E, Moser MB, Moser EI. 2008. Representation of geometric borders in the entorhinal cortex. Science 322(5909):1865-1868.
Stanton GB, Cruce WL, Goldberg ME, Robinson DL. 1977. Some ipsilateral projections to areas PF and PG of the inferior parietal lobule in monkeys. Neurosci Lett 6(2-3):243-250.
Steffenach HA, Witter M, Moser MB, Moser EI. 2005. Spatial memory in the rat requires the dorsolateral band of the entorhinal cortex. Neuron 45(2):301-313.
Stepniewska I, Friedman RM, Gharbawie OA, Cerkevich CM, Roe AW, Kaas JH. 2011. Optical imaging in galagos reveals parietal-frontal circuits underlying motor behavior. Proceedings of the National Academy of Sciences of the United States of America 108(37):E725-732.
Sugar J, Witter MP. 2016. Postnatal development of retrosplenial projections to the parahippocampal region of the rat. eLife 5:e13925.
Sugar J, Witter MP, van Strien NM, Cappaert NL. 2011. The retrosplenial cortex: intrinsic connectivity and connections with the (para)hippocampal region in the rat. An interactive connectome. Frontiers in neuroinformatics 5(Article 7).
Suzuki WA, Amaral DG. 1994. Perirhinal and parahippocampal cortices of the macaque monkey: cortical afferents. J Comp Neurol 350(4):497-533.
Swanson LW, Kohler C. 1986. Anatomical evidence for direct projections from the entorhinal area to the entire cortical mantle in the rat. J Neurosci 6(10):3010-3023.
Taube JS. 1995. Place cells recorded in the parasubiculum of freely moving rats. Hippocampus 5(6):569-583.
Taube JS, Kesslak JP, Cotman CW. 1992. Lesions of the rat postsubiculum impair performance on spatial tasks. Behav Neural Biol 57(2):131-143.

Taube JS, Muller RU, Ranck JB, Jr. 1990a. Head-direction cells recorded from the postsubiculum in freely moving rats. I. Description and quantitative analysis. J Neurosci 10(2):420-435.
Taube JS, Muller RU, Ranck JB, Jr. 1990b. Head-direction cells recorded from the postsubiculum in freely moving rats. II. Effects of environmental manipulations. J Neurosci 10(2):436-447.
van Groen T, Wyss JM. 1990a. The connections of presubiculum and parasubiculum in the rat. Brain Res 518(1-2):227-243.
van Groen T, Wyss JM. 1990b. Connections of the retrosplenial granular a cortex in the rat. J Comp Neurol 300(4):593-606.
van Groen T, Wyss JM. 1990c. The postsubicular cortex in the rat: characterization of the fourth region of the subicular cortex and its connections. Brain Res 529(1-2):165-177.
van Groen T, Wyss JM. 1992. Connections of the retrosplenial dysgranular cortex in the rat. J Comp Neurol 315(2):200-216.
Van Groen T, Wyss JM. 2003. Connections of the retrosplenial granular b cortex in the rat. J Comp Neurol 463(3):249-263.
van Haeften T, Wouterlood FG, Jorritsma-Byham B, Witter MP. 1997. GABAergic presubicular projections to the medial entorhinal cortex of the rat. J Neurosci 17(2):862-874.
Vogt BA, Miller MW. 1983. Cortical connections between rat cingulate cortex and visual, motor, and postsubicular cortices. J Comp Neurol 216(2):192-210.
Whitlock JR. 2014. Navigating actions through the rodent parietal cortex. Front Hum Neurosci 8(Article 293).
Whitlock JR, Pfuhl G, Dagslott N, Moser MB, Moser EI. 2012. Functional split between parietal and entorhinal cortices in the rat. Neuron 73(4):789-802.
Whitlock JR, Sutherland RJ, Witter MP, Moser MB, Moser EI. 2008. Navigating from hippocampus to parietal cortex. Proceedings of the National Academy of Sciences of the United States of America 105(39):14755-14762.
Wilber A, Clark BJ, Demecha AJ, Mesina L, Vos JM, McNaughton BL. 2015. Cortical Connectivity Maps Reveal Anatomically Distinct Areas in the Parietal Cortex of the Rat. Frontiers in Neural Circuits 8(Article 146).
Wilber AA, Clark BJ, Forster TC, Tatsuno M, McNaughton BL. 2014. Interaction of egocentric and world-centered reference frames in the rat posterior parietal cortex. J Neurosci 34(16):5431-5446.
Witter MP, Chan-Palay V, Köhler C. 1989. Connectivity of the rat hippocampus. In: Chan-Palay V, Köhler C, eds. The Hippocampus - New Vistas. Neurol. Neurobiol. New York: Allan Liss, inc. p 53-69.
Wyss JM, Van Groen T. 1992. Connections between the retrosplenial cortex and the hippocampal formation in the rat: a review. Hippocampus 2(1):1-11.

## Acknowledgements

The authors are grateful to Hanna Haaland Sømme and Karoline Hovde for providing some of the experimental cases, and to Bruno Monterotti and Paulo Girão for their excellent technical assistance in sectioning and histological processing of parts of the material. We are further thankful to Jonathan Whitlock for valuable comments on the manuscript.

**Figures**

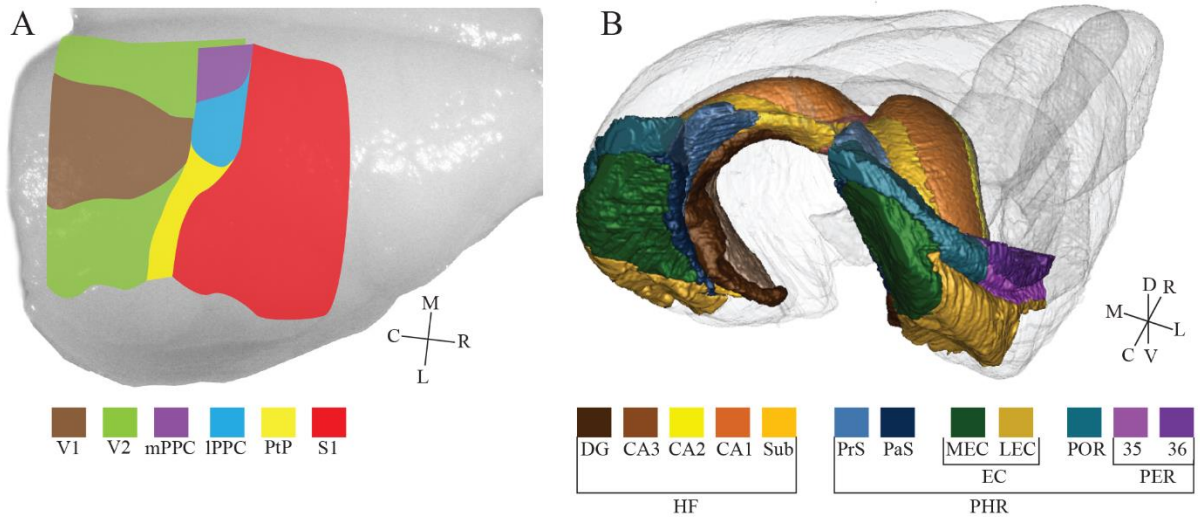


**Figure 1. Cortical delineations.** Schematic representation of the position and subdivision of the caudal association cortex (A) and PHR (B) in rat, according to Olsen and Witter (2016) and Boccara et al. (2015), respectively.

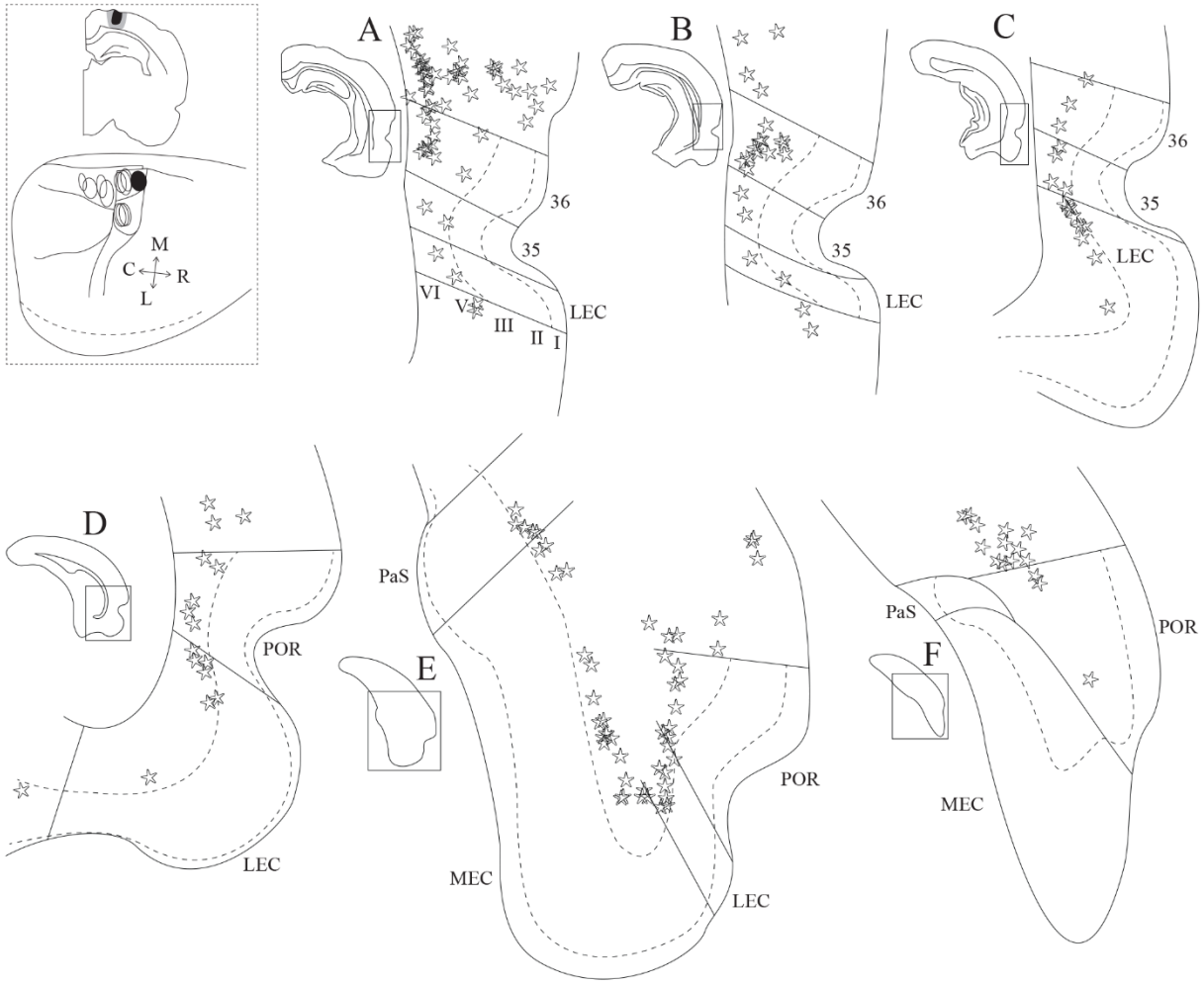


**Figure 2. PHR input to mPPC.** Retrogradely labeled cells in the PHR, represented by open stars, after injection of Fast Blue in mPPC. A-F: Series of coronal sections arranged from rostral to caudal, showing higher magnifications of the boxed area of PHR. Solid black lines represent borders between parahippocampal areas, while dashed lines represent borders between layers I and II/III, and between layers II/III and V/VI. Dense labeling is present in deep layers of PER areas 35 and 36 as well as POR, in addition to adjacent parts of LEC and MEC. Inset, top: outline of the injection site in a coronal section of the brain. The black filled region represents the core of the injection while the gray filled region represents the full lateral extent. Inset,

bottom: the core of the injection site is represented with a black filled circle in a dorsal rendering of the caudal cortex. Open circles represent other retrograde tracer injections investigated in this study. Black lines indicate borders between areas of the cortex as outlined in Figure 1a.

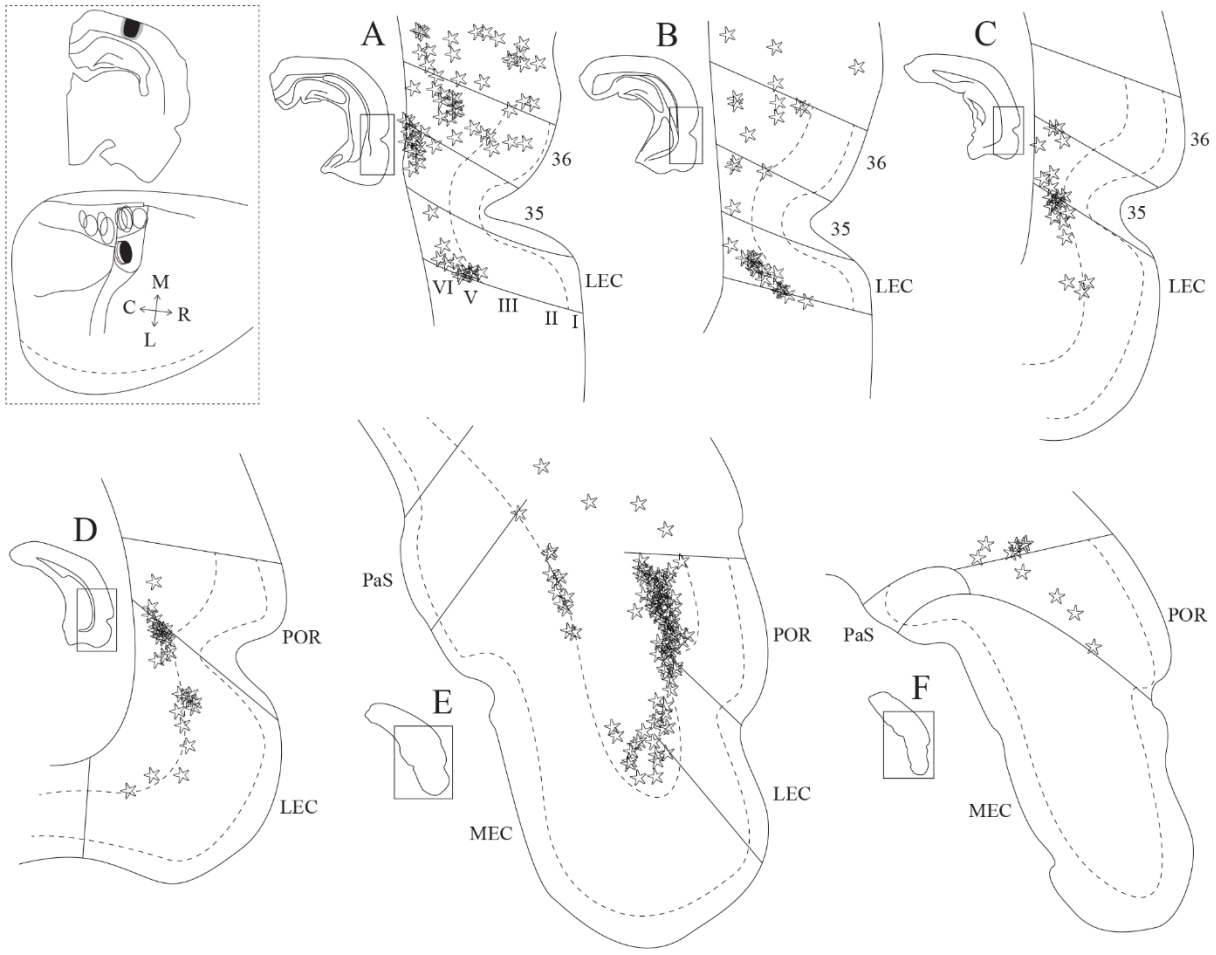


**Figure 3. PHR input to lPPC.** Retrogradely labeled cells in the PHR, represented by open stars, after injection of Fast Blue in lPPC. A-F: Series of coronal sections arranged from rostral to caudal, showing higher magnifications of the boxed area of PHR. Solid black lines represent borders between parahippocampal areas, while dashed lines represent borders between layers I and II/III, and between layers II/III and V/VI. The majority of labeled cells are located in deep layers and are found in PER areas 35 and 36 as well as POR, in addition to adjacent parts of LEC and MEC. Inset, top: outline of the injection site in a coronal section of the brain. The black filled region represents the core of the injection while the gray filled region represents the full lateral extent. Inset, bottom: the core of the injection site is represented with a black filled circle

in a dorsal rendering of the caudal cortex. Open circles represent other retrograde tracer injections investigated in this study. Black lines indicate borders between areas of the cortex as outlined in Figure 1a.

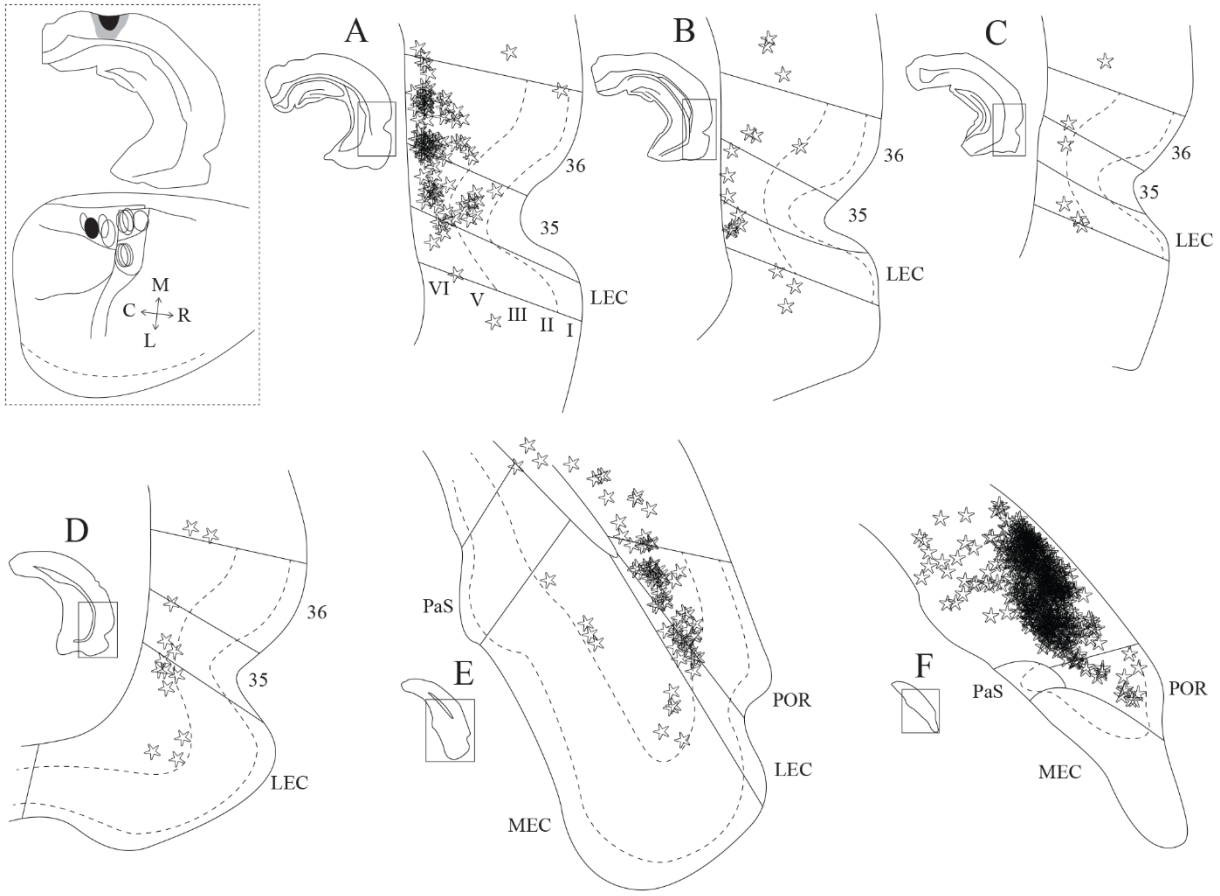


**Figure 4. PHR input to V2M.** Retrogradely labeled cells in the PHR, represented by open stars, after injection of Fast Blue in V2M. A-F: Series of coronal sections arranged from rostral to caudal, showing higher magnifications of the boxed area of PHR. Solid black lines represent borders between parahippocampal areas, while dashed lines represent borders between layers I and II/III, and between layers II/III and V/VI. Dense labeling is present in deep layers of PER areas 35 and 36 as well as POR, in addition to adjacent parts of LEC and MEC. Inset, top: outline of the injection site in a coronal section of the brain. The black filled region represents the core of the injection while the gray filled region represents the full lateral extent. Inset, bottom: the core of the injection site is represented with a black filled circle in a dorsal rendering

of the caudal cortex. Open circles represent other retrograde tracer injections investigated in this study. Black lines indicate borders between areas of the cortex as outlined in Figure 1a.

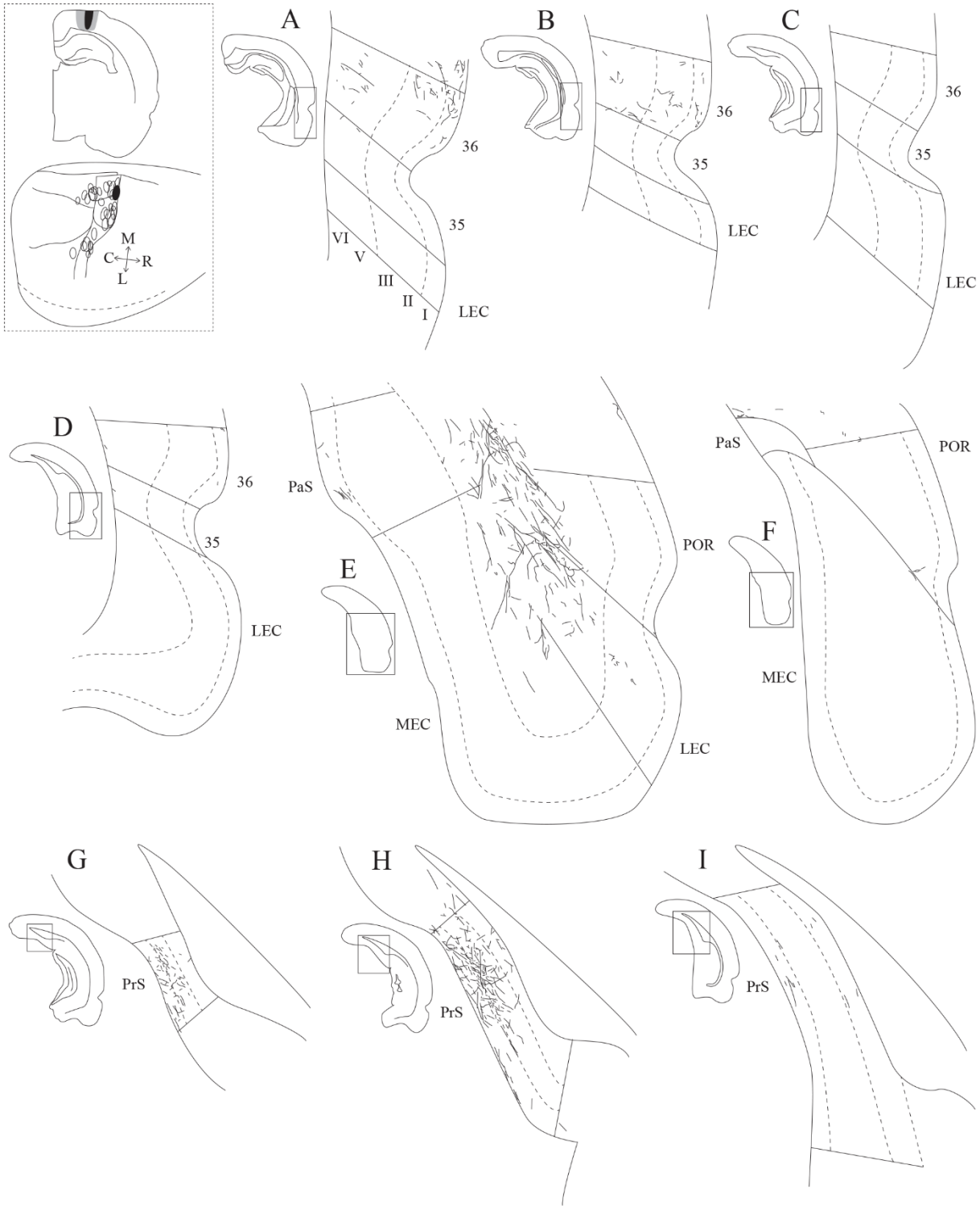


**Figure 5. mPPC projections to PHR.** Anterograde labeling in the PHR after an injection of PHA-L in mPPC. A-I: Series of coronal sections arranged from rostral to caudal, showing higher

magnifications of the boxed area of PHR. Solid black lines represent borders between parahippocampal areas, while dashed lines represent borders between layers I and II/III, and between layers II/III and V/VI. Labeled fibers are concentrated rostrally in PER, deep layers of POR and caudal EC, as well as layers I and III of dorsal PrS, some fibers are also located in layer I of PaS. Inset, top: outline of the injection site in a coronal section of the brain. The black filled region represents the core of the injection while the gray filled region represents the full lateral extent. Inset, bottom: the core of the injection site is represented with a black filled circle in a dorsal rendering of the caudal cortex. Open circles represent other retrograde tracer injections investigated in this study. Black lines indicate borders between areas of the cortex as outlined in Figure 1a.

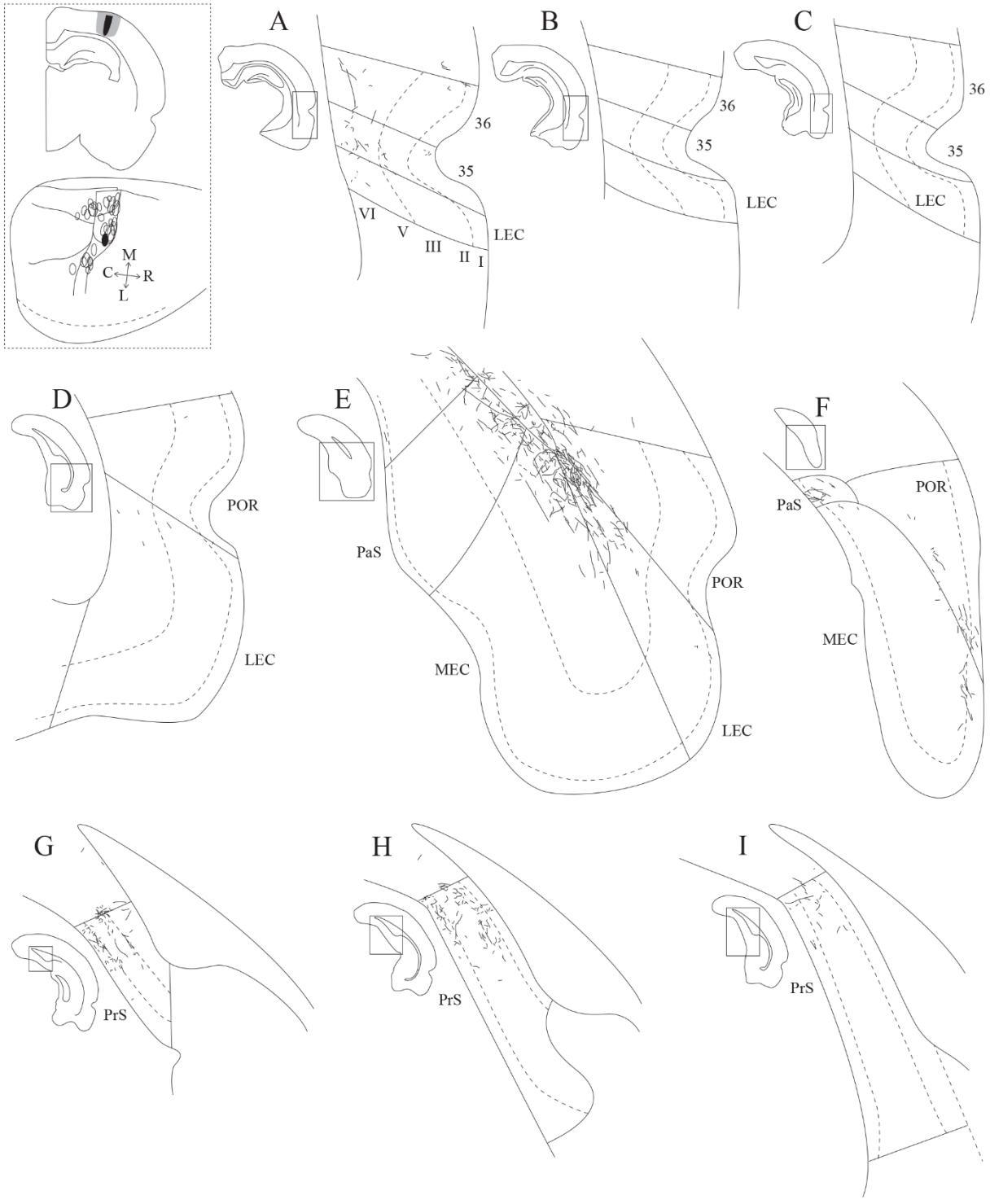


**Figure 6. lPPC projections to PHR.** Anterograde labeling in the PHR after an injection of PHA-L in lPPC. A-I: Series of coronal sections arranged from rostral to caudal, showing higher magnifications of the boxed area of PHR. Solid black lines represent borders between

parahippocampal areas, while dashed lines represent borders between layers I and II/III, and between layers II/III and V/VI. Labeled fibers are focused rostrally in PER, deep layers of POR and caudal EC, as well as layers I and III of dorsal PrS and layer I of caudal PaS. Inset, top: outline of the injection site in a coronal section of the brain. The black filled region represents the core of the injection while the gray filled region represents the full lateral extent. Inset, bottom: the core of the injection site is represented with a black filled circle in a dorsal rendering of the caudal cortex. Open circles represent other retrograde tracer injections investigated in this study. Black lines indicate borders between areas of the cortex as outlined in Figure 1a.

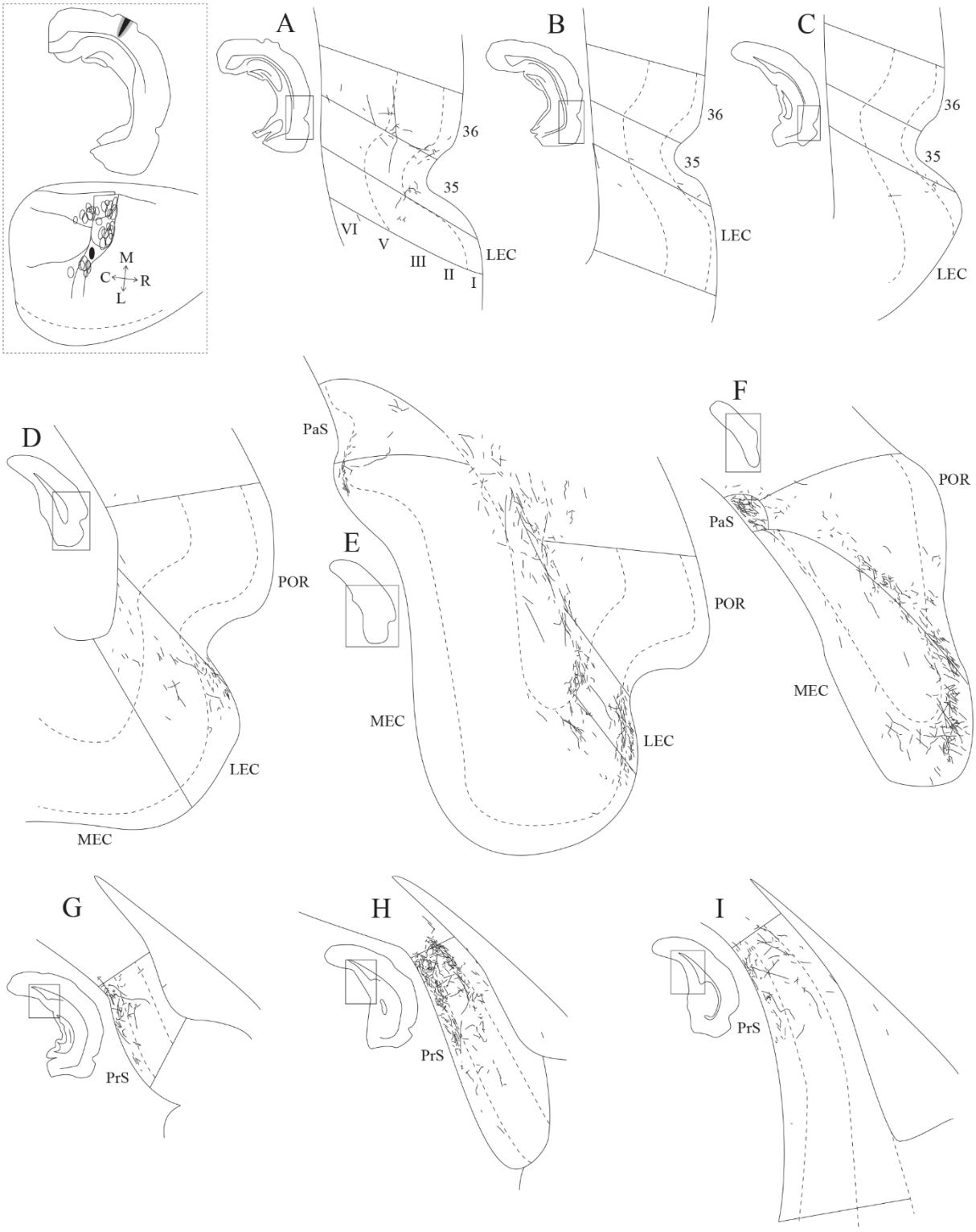


**Figure 7. PtP projections to PHR.** Anterograde labeling in the PHR after an injection of PHA-L in PtP. A-I: Series of coronal sections arranged from rostral to caudal, showing higher

magnifications of the boxed area of PHR. Solid black lines represent borders between parahippocampal areas, while dashed lines represent borders between layers I and II/III, and between layers II/III and V/VI. Labeled fibers are concentrated rostrally in PER, deep layers of POR, layers I, III and V of caudal EC, as well as layers I and III of dorsal PrS and layer I of caudal PaS. Inset, top: outline of the injection site in a coronal section of the brain. The black filled region represents the core of the injection while the gray filled region represents the full lateral extent. Inset, bottom: the core of the injection site is represented with a black filled circle in a dorsal rendering of the caudal cortex. Open circles represent other retrograde tracer injections investigated in this study. Black lines indicate borders between areas of the cortex as outlined in Figure 1a.

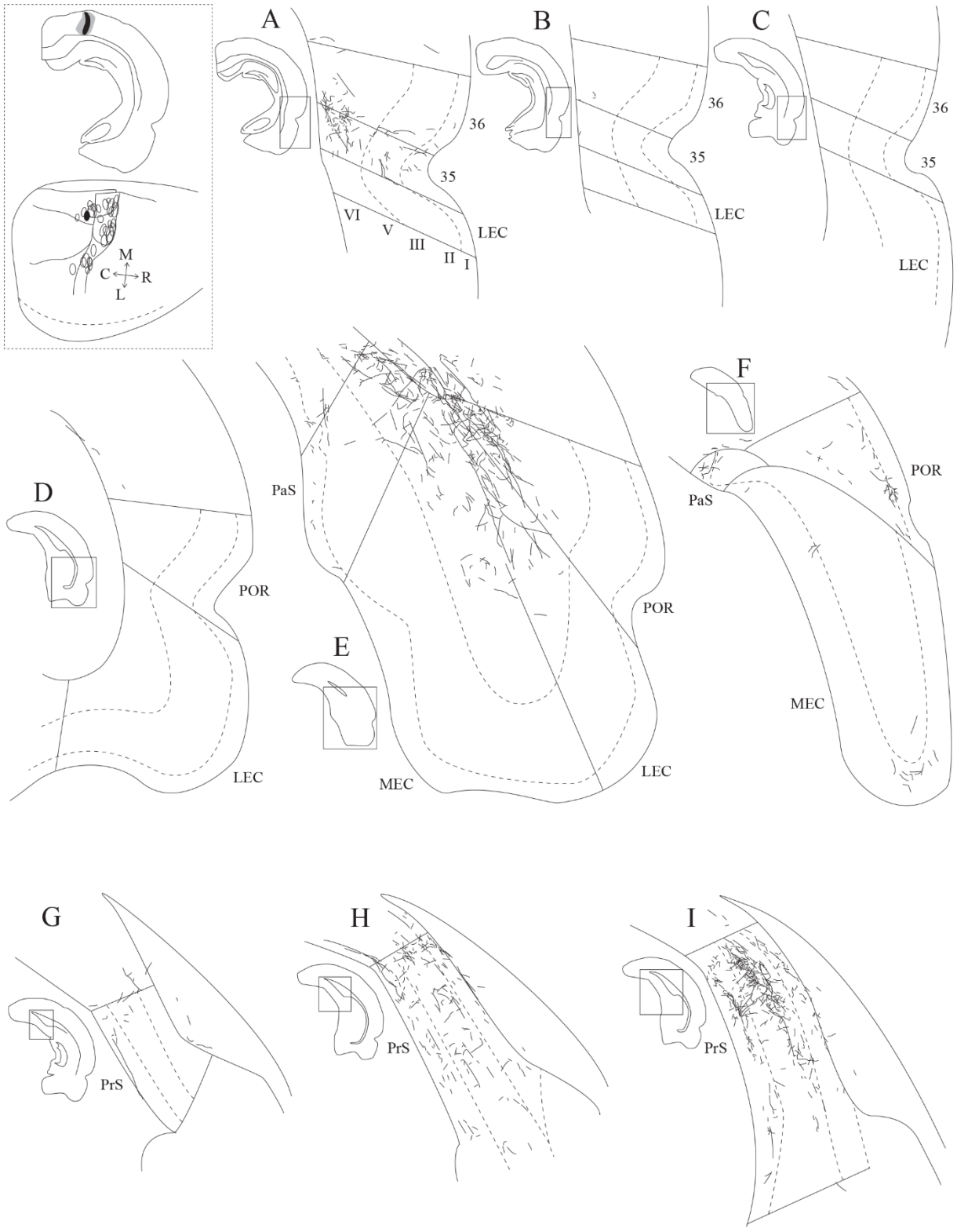
A
B
C
36
35
LEC
VI
V
III
II
I
M
C
R
L
D
POR
LEC
PaS
E
MEC
F
G
PrS
H
I

**Figure 8. V2M projections to PHR.** Anterograde labeling in the PHR after an injection of PHA-L in V2M. A-I: Series of coronal sections arranged from rostral to caudal, showing higher magnifications of the boxed area of PHR. Solid black lines represent borders between parahippocampal areas, while dashed lines represent borders between layers I and II/III, and between layers II/III and V/VI. Labeled fibers are located rostrally in PER 36, layer VI and I of POR and caudal EC, as well as layers I and III of PrS and layer I of PaS. Inset, top: outline of the injection site in a coronal section of the brain. The black filled region represents the core of the injection while the gray filled region represents the full lateral extent. Inset, bottom: the core of the injection site is represented with a black filled circle in a dorsal rendering of the caudal cortex. Open circles represent other retrograde tracer injections investigated in this study. Black lines indicate borders between areas of the cortex as outlined in Figure 1a.

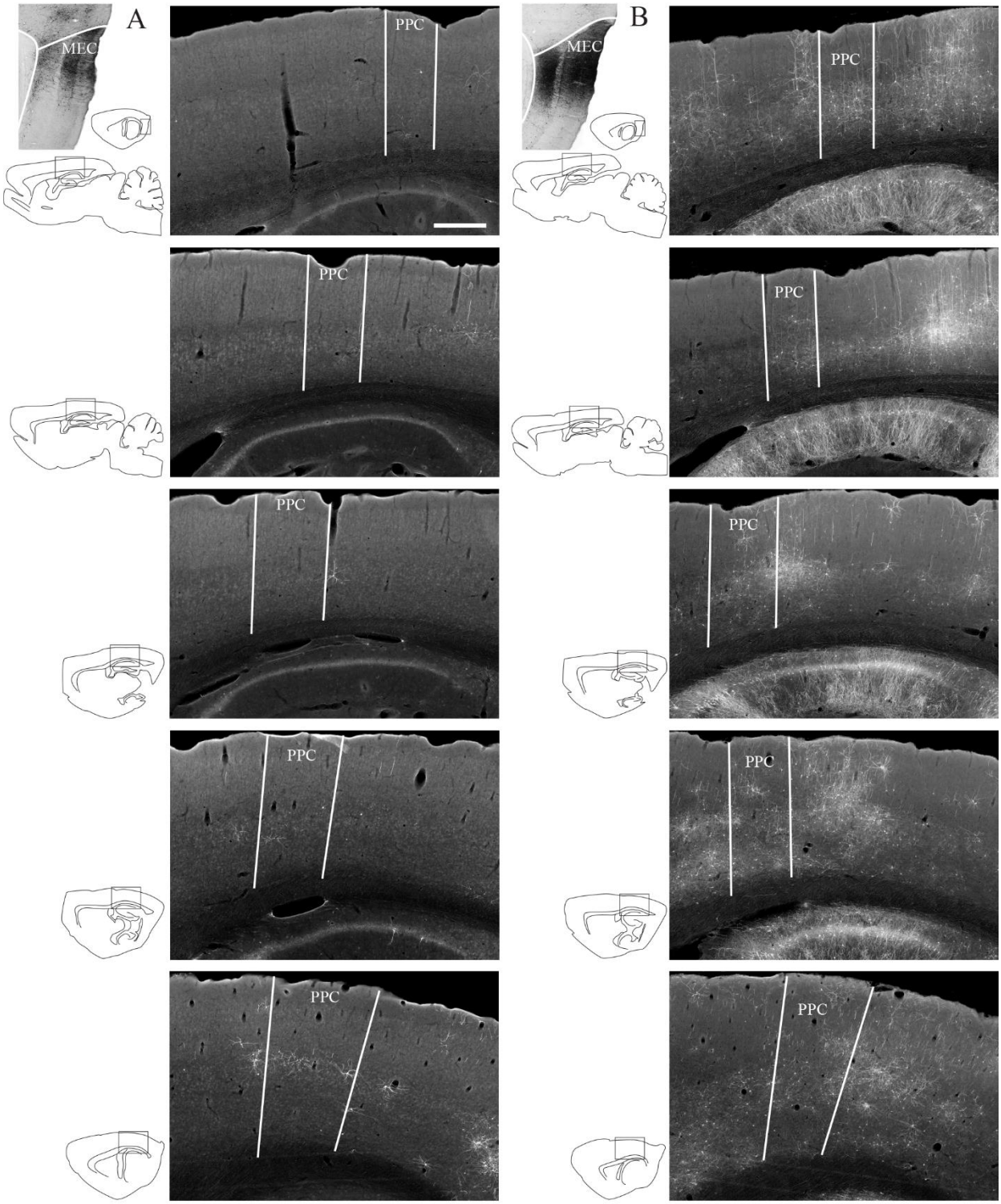


**Figure 9. Direct and transsynaptic PPC input to PHR.** Pseudo-darkfield images of sagittal sections arranged from medial (top) to lateral (bottom) containing retrogradely labeled neurons

in the cortex after injections of a modified rabies virus in MEC at a survival time of two (A) or five (B) days, allowing for mono- and disynaptic tracing, respectively. Note the very low number of labeled neurons in PPC after two days (A) and the increased number of labeled cells after five days (B). Scalebar 500 µm.

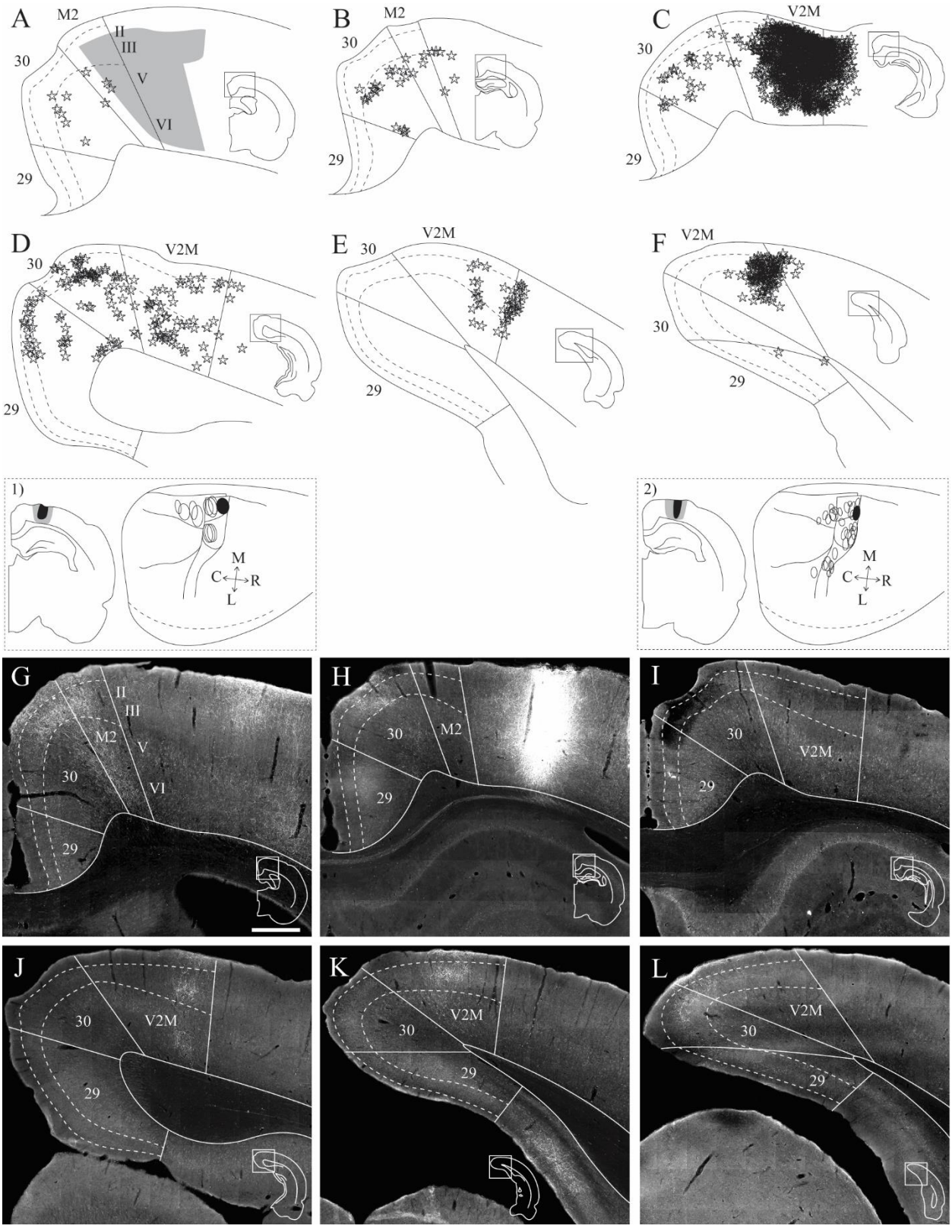
A
M2
II
III
V
VI
30
29
B
M2
30
29
C
V2M
30
29
D
V2M
30
29
E
V2M
30
29
F
V2M
30
29
1)
M
C
R
L
2)
M
C
R
L
G
II
III
M2
V
VI
30
29
H
30
M2
29
I
30
V2M
29
J
30
V2M
29
K
V2M
30
29
L
V2M
30
29

**Figure 10. mPPC-RSC connections.** Labeling in RSC after injection of a retrograde tracer (Fast Blue, inset 1, panels A-F) or an anterograde tracer (PHA-L, inset 2, panels G-L) in mPPC. A-F and G-L: Series of coronal sections arranged from rostral to caudal, showing higher magnifications of the boxed area of RSC. Solid lines represent borders between retrosplenial and neighboring areas, while dashed lines represent borders between layers I and II/III, and between layers II/III and V/VI. Labeling is prominent in rostral area 30. In A, the filled gray outline represents very dense clustering of labeled cells in caudal M2 and the adjacent M1. Insets show the injection sites in a coronal section and a rendering of the dorsal caudal cortex as outlined in Figure 1a, where the black filled outline represents the core of the injection site. Scalebar (in G) 500 μm.

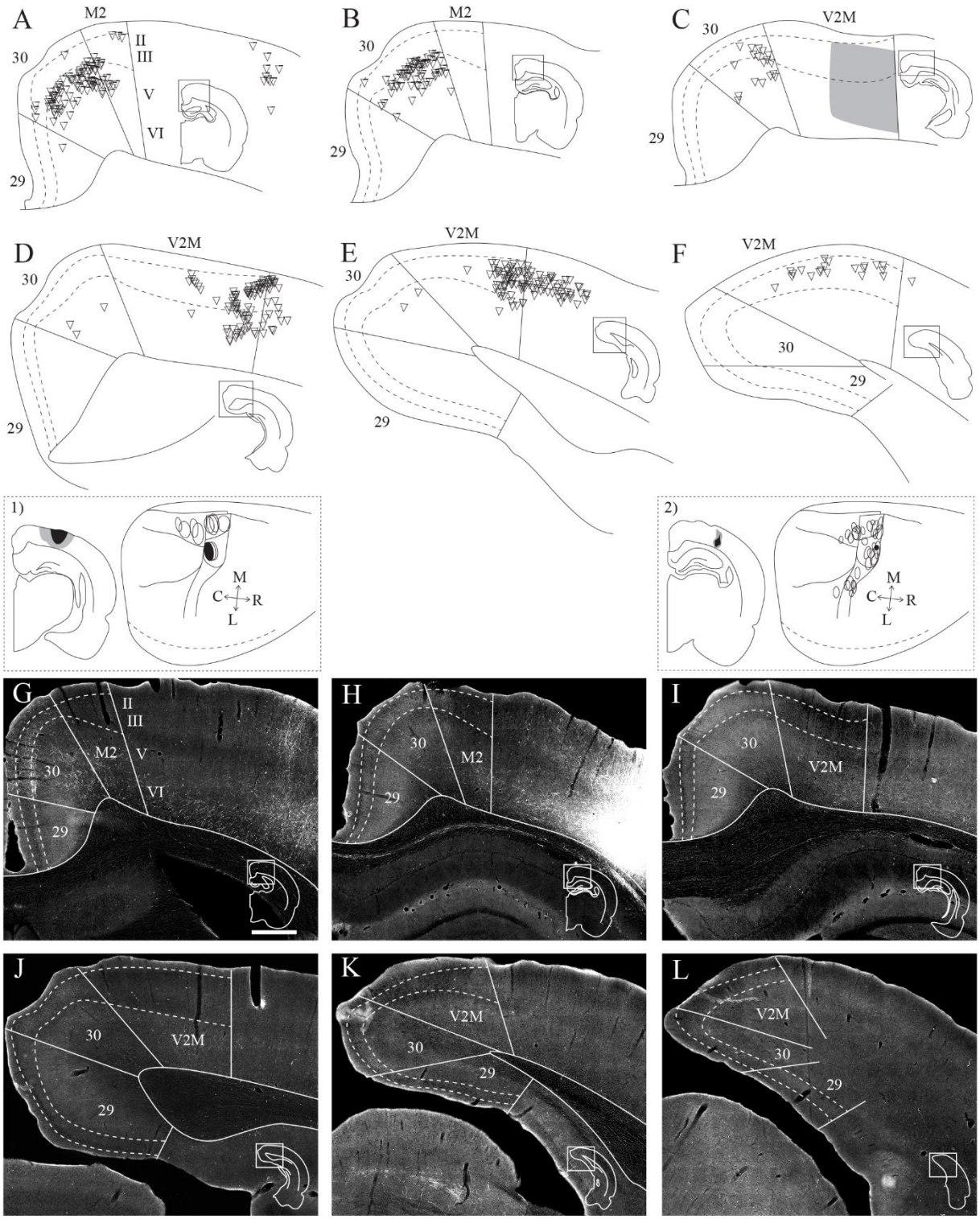


**Figure 11. lPPC-RSC connections.** Labeling in RSC after injection of a retrograde tracer (Fluorogold, inset 1, panels A-F) or an anterograde tracer (BDA, inset 2, panels G-L) tracer in

lPPC. A-F and G-L: Series of coronal sections arranged from rostral to caudal, showing higher magnifications of the boxed area of RSC. Solid lines represent borders between retrosplenial and neighboring areas, while dashed lines represent borders between layers I and II/III, and between layers II/III and V/VI. Labeling is focused particularly rostrally in area 30. In C, the filled gray outline represents a dense cluster of labeled cells in V2M. Insets show the injection sites in a coronal section and a rendering of the dorsal caudal cortex as outlined in Figure 1a, where the black filled outline represents the core of the injection site. Scalebar (in G) 500 μm.

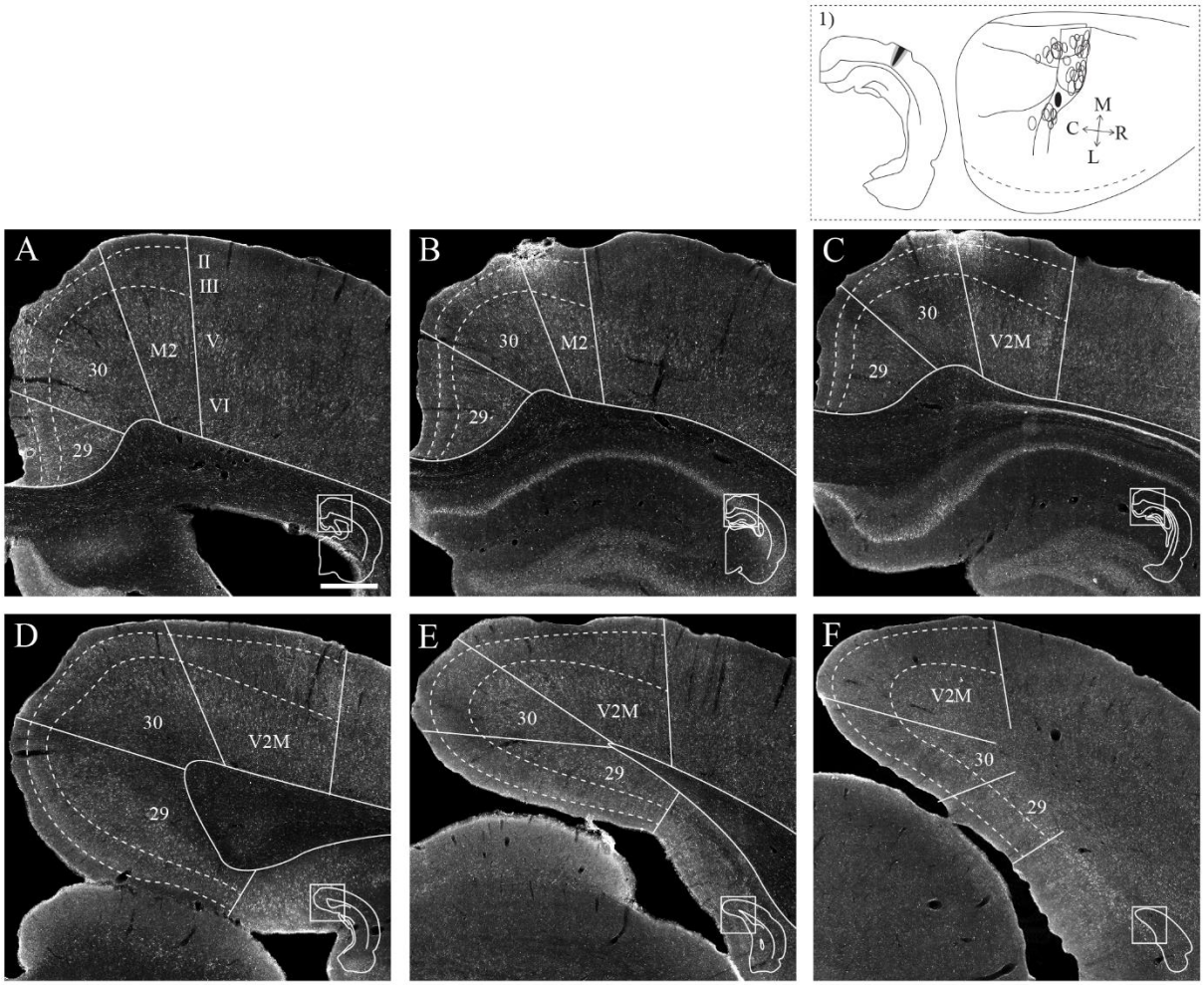


**Figure 12. PtP-RSC projections.** Labeling in RSC after injection of an anterograde tracer (PHA-L) in PtP. A-F: Series of coronal sections arranged from rostral to caudal, showing higher magnifications of the boxed area of RSC. Solid lines represent borders between retrosplenial and neighboring areas, while dashed lines represent borders between layers I and II/III, and between layers II/III and V/VI. Labeling is most concentrated in rostral area 30. Insets show the injection sites in a coronal section and a rendering of the dorsal caudal cortex as outlined in Figure 1a, where the black filled outline represents the core of the injection site. Scalebar (in A) 500 µm.

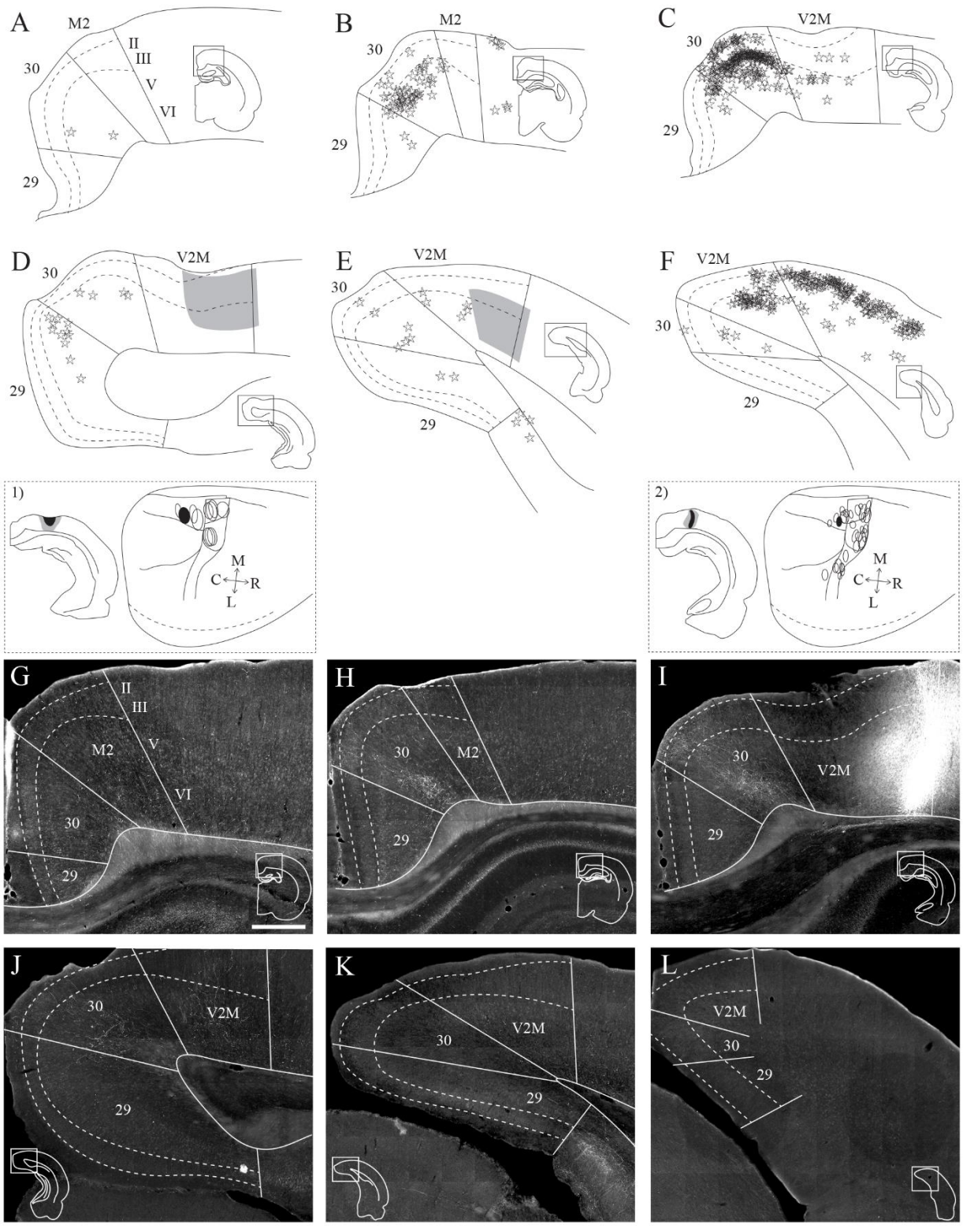
A
M2
II
III
V
VI
30
29
B
M2
30
29
C
V2M
30
29
D
V2M
30
29
E
V2M
30
29
F
V2M
30
29
1)
M
C
R
L
2)
M
C
R
L
G
II
III
M2
V
VI
30
29
H
30
M2
29
I
30
V2M
29
J
30
V2M
29
K
V2M
30
29
L
V2M
30
29

**Figure 13. V2M-RSC connections.** Labeling in RSC after injection of a retrograde tracer (Fast Blue, inset 1, panels A-F) or an anterograde tracer (PHA-L, inset 2, panels G-L) tracer in V2M. A-F and G-L: Series of coronal sections arranged from rostral to caudal, showing higher magnifications of the boxed area of RSC. Solid lines represent borders between retrosplenial and neighboring areas, while dashed lines represent borders between layers I and II/III, and between layers II/III and V/VI. Labeling is prominent in area 30. In D and E, the filled gray outline represents very dense clustering of labeled cells in the lateral portion of V2M. Insets show the injection sites in a coronal section and a rendering of the dorsal caudal cortex as outlined in Figure 1a, where the black filled outline represents the core of the injection site. Scalebar (in G) 500 μm.

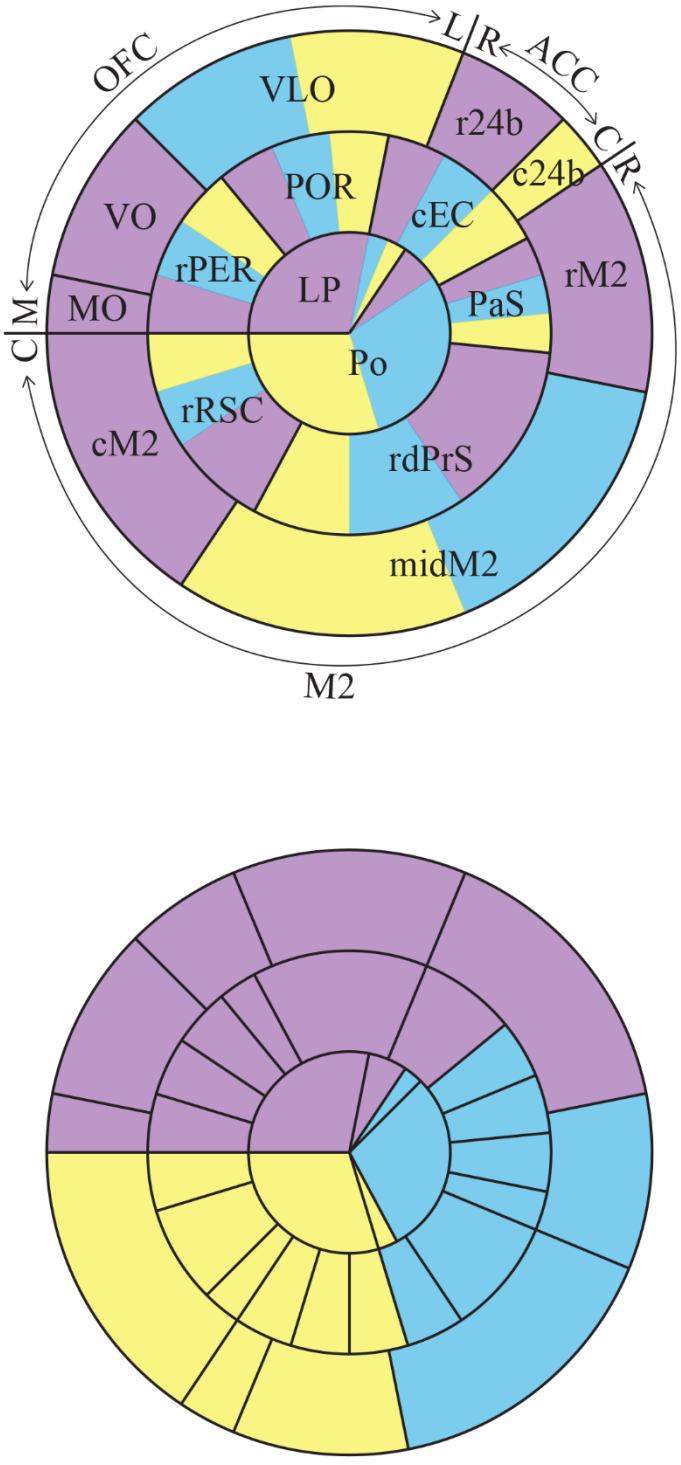


**Figure 14. Diagram of parietal-parahippocampal projections.** The center of the circle shows a colorcoded representation of the three PPC subdivisions, mPPC (purple), lPPC (blue), and PtP

(yellow), separated with black lines. The outer circle represents the relative proportion of projections, indicated by the size of the colorcoded areas, from the three PPC subdivisions to the parahippocampal areas which are separated with black lines. rPER, rostral PER; cEC, caudal EC; cPaS, caudal PaS; rdPrS, rostrodorsal PrS; r30, rostral area 30.

**List of abbreviations**

*Cortical areas*

Area 29 – retrosplenial area 29

Area 30 – retrosplenial area 30

Area 35 – perirhinal area 35

Area 36 – perirhinal area 36

EC – entorhinal cortex

LEC – lateral entorhinal cortex

lPPC – lateral posterior parietal cortex

M2 – secondary motor cortex

MEC – medial entorhinal cortex

mPPC – medial posterior parietal cortex

PaS – parasubiculum

PER – perirhinal cortex

PHR – parahippocampal region

POR – postrhinal cortex

PPC – posterior parietal cortex

PrS – presubiculum

PtP – caudal part of posterior parietal cortex

RSC – retrosplenial cortex

V2 – secondary visual cortex

V2L – lateral secondary visual cortex

V2M – medial secondary visual cortex

*Others*

I-VI – cortical layers of PHR

ABC – avidin-biotin complex

BDA – biotinylated dextran amine

C or c – caudal

DAB – 3,3’-diaminobenzidine tetrahydrochloride

DMSO – dimethyl sulfoxide

EGFP – enhanced green fluorescent protein

GFP – green fluorescent protein

L or l – lateral

M or m – medial

PBS – phosphate buffered saline

PBT – phosphate buffered saline with Triton X-100

PHA-L – *phaseolus vulgaris* leucoagglutinin

R or r – rostral